PARTICLE PHYSICS DIVISION

PHYSICS DEPARTMENT

LUND UNIVERSITY

2012

Elliptic Flow of K^0_s's, Λ's and $\bar{\Lambda}$'s in Pb-Pb 20-40% Central collisions at $\sqrt{s_{NN}} = 2.76TeV$ measured with the ALICE Detector at LHC

Bachelor's thesis submitted for the 15-ECTS Bachelor´s Degree

Project Program FYSK01 under authorization of

LUND UNIVERSITY, SWEDEN

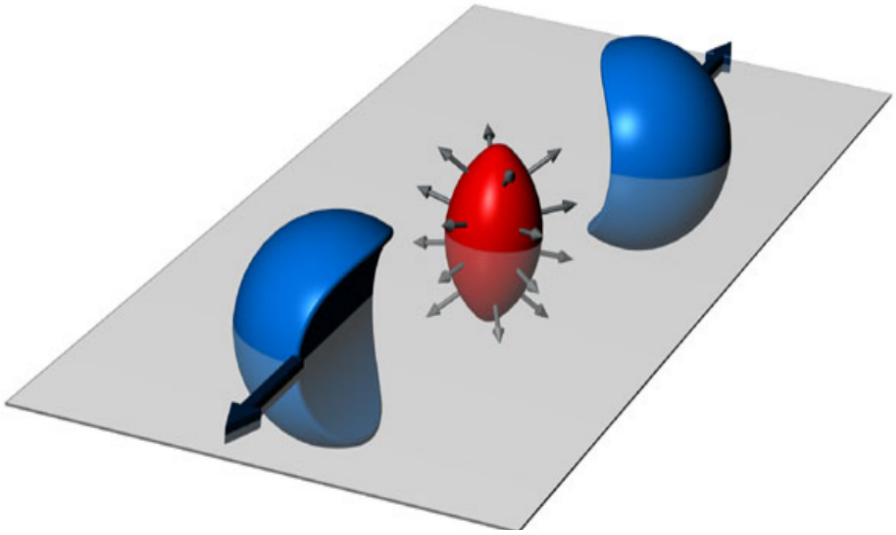

Georgios Krintiras

Supervisor:Peter Christiansen

Abstract

We report measurement of elliptic flow $v_2(p_T)$ in extended transverse momentum range for the identified cases of K^0_s (< 8.5GeV/c), Λ and $\bar{\Lambda}$ (< 7.5GeV/c) in Pb$-$Pb 20-40% central collisions at $\sqrt{s_{NN}} = 2.76$ TeV measured with the ALICE detector at LHC. While K^0_s's reach a maximum of $v_2 = 0.167 \pm 0.0007(stat)$ at $p_T \approx 3$Gev/c, the baryon (anti-baryon) $v_2(p_T)$ continues to rise until it reaches a maximum of $v_2(p_T) = 0.213 \pm 0.0013(stat)(0.214 \pm 0.0014(stat))$ at $p_T \approx 4$GeV/c. For larger p_T, the $v_2(p_T)$ values exhibit a gradual decrease for all three cases. Quark scaling properties are also examined, indicating that at intermediate and high p_T scaling does not hold for strange particles $v_2(p_T)$.

Georgios Krintiras

Elliptiskt flöde av K^0_s, Λ's och $\bar{\Lambda}$'s i bly-bly-kollisioner med 20-40% centralitet vid energin $\sqrt{s_{NN}}$=2.76TeV mätt med ALICE detektorn vid LHC

Ultrarelativistiska kollisioner mellan tunga kärnor skapar en så kallad kvark–gluon-plasma (QGP), vilket är ett materia-tillstånd där kvarkar och gluoner anses "fria" (de är inte bundna till varandra av den starka kraften för att utgöra hadroner). ALICE vid LHC är ett tungjons-orienterat experiment, vars syfte är att utforska just kvark-gluon-plasma genom att kollidera Pb-208 med en energi av $\sqrt{s_{NN}} = 2.76$ TeV per nukleon i masscentret. Kollisionens centralitet bestäms av de laddade partiklarnas multiplicitet (antal producerade partiklar) och följer den allmänna regeln att ju högre multipliciteten är, desto mer central är kollisionen.

I icke-centrala kollisioner beskriver bly-kärnornas överlappande regioner en ellipsoid. Denna spatiella anasotropi som är störst i kollisionens inledande utveckling umvandlas genom växelverkan bland systemets beståndsdelar till en anasitropi i partiklarnas rörelsemängd; man pratar om att systemet "flödar" (på engelska *flow*). Genom att mäta flödet och växelverkan mellan partiklarna kan man ernälla information om kollisionernas tidiga skede.

Från lågenergetiska experiment med s.k. *fixed target*, till relativistiskt högenergetiska kollisioner – tidigare vid RHIC och nu vid LHC – är partiklars flöde en spännande aspekt som avslöjar dynamiken i utvecklingen hos ett system. Dess transversa komponent beskriver den azimutala anisotropin av icke-centrala kollisioners partikel-emission, i planet vinkelrätt mot kollisions-strålarnas riktning. Ett bekvämt sätt att beskriva olika former av anisotropiskt flöde är genom att använda sig av en Fourier-utveckling av den azimutala rörelsemängds-fördelningen; den andra harmoniska koefficienten, $v_2(p_T, y)$, beskriver således ett elliptiskt mönster.

Standardmetoden för att rekonstruera reaktions-planet har delvis behandlats i uppsatsen, genom att beräkna vinkeln av andra ordningens symmetriplan, Ψ_2. En statistisk behandling har använts för att extrahera $v_2(p_T)$ parametrar från den transversa rörelsemängden och den invarianta mass-fördelningen för laddade partiklar och identifierade partiklar. Giltigheten av den förenklat inbyggda metoden styrks genom en jämförelse med resultat från ATLAS analys av elliptiskt flöde. Även om p_T-beroendet av v_2 följer det mönster som observerats vid RHIC, är partikeltypens p_T-beroende i rak motsats till den s.k. *quark coalescence*-modellen där det är valenskvarkar som flödar.

Handledare: **Peter Christiansen**
15-Hp Kandidatarbete, FYSK01
Institutionen för fysik, Lunds universitet

Contents

1 Introduction **6**

2 Elliptic Transverse Flow: Definition and Analysis Methods **7**

3 Fourier Expansion of Azimuthal Particle Distributions **8**

4 Reaction Plane Estimation– The Event Plane Method **10**

5 Analysis **11**
5.1 Extracting the Reaction Plane and Elliptic Flow of Charged Particles 11
5.2 Anisotropy parameter $v_2(p_T)$ for K^0_s, Λ and $\bar{\Lambda}$; mass *splitting* and quark scaling 12

6 Results **15**

7 Discussion **16**

8 Acknowledgements **18**

A APPENDIX **19**
A.1 Collision Geometry and Source Eccentricity 20
A.2 Kinematic Variables 20
A.3 Multiplicity and centrality 21
A.4 Vertex topology and V^0 selection criteria 24
A.5 The Data 24
A.6 Figures 25

List of Figures

2.1 Transverse view of the initial overlap region and conversion from coordinate space into momentum space 7
2.2 Charged hadron v_2 integrated over p_T and η as a function of centrality for various methods 8
3.1 Ellipse-like distribution in polar coordinates 10
3.2 A simulated Pb-Pb collision at $\sqrt{s_{NN}} = 2.76TeV$ 10
5.1 Distributions of $\bar{\Lambda}$, Λ and K_s^0 candidates in the $\Delta m - (\phi_{lab} - \Psi_2)$ plane 14
5.2 Anisotropy parameter $v_2(p_T)$ for K_s^0,Λ and$\bar{\Lambda}$ 14
5.3 Anisotropy parameter $v_2(p_T/n)$ for K_s^0,Λ and$\bar{\Lambda}$ 15
A.1 A heavy ion collision seen from the (CM) frame 19
A.2 Spectators and participants 19
A.3 Coordinate system for the transverse plane in heavy ion collisions 20
A.4 Flow coordinate system 21
A.5 Charged particle multiplicity at different energies and for different collision system 22
A.6 Charged particle multiplicity for different centrality classes 22
A.7 Integrated charged particle multiplicity 23
A.8 Centrality determination in ALICE 23
A.9 V^0 vertex topology 24
A.10 Azimuthal distribution of the event plane based on DATA set 1 25
A.11 Azimuthal distribution of the event plane based on DATA set 2 26
A.12 Azimuthal distributions with respect to the reconstructed reaction plane Ψ_2 momentum 27
A.13 Distribution of the azimuthal angle relative to the measured event plane angle in eight centrality intervals for $2 \leq p_T \leq 2.5GeV$. 28
A.14 Distribution of the azimuthal angle relative to the measured event plane angle in eight centrality intervals for $5 \leq p_T \leq 5.5GeV$. 29
A.15 Distribution of the azimuthal angle relative to the measured event plane angle in eight centrality intervals for $10.5 \leq p_T \leq 11GeV/c$. 30
A.16 Elliptic flow $v_2(p_T)$ as a function of p_T for eight 10% centrality intervals, for p_T from 0.5 to 20 GeV/c 31
A.17 Azimuthal distributions with respect to the reconstructed reaction plane Ψ_2 invariant mass distributions for $\bar{\Lambda}$ 32
A.18 Azimuthal distributions with respect to the reconstructed reaction plane Ψ_2 invariant mass distributions for Λ hyperons 33
A.19 Azimuthal distributions with respect to the reconstructed reaction plane Ψ_2 invariant mass distributions for K_s^0 mesons 34
A.20 Invariant mass fitting for $\bar{\Lambda}$ near 0 rad 35
A.21 Invariant mass fitting for Λ near 0 rad 36
A.22 Invariant mass fitting for K_s^0 near 0 rad 37
A.23 Number of produced $\bar{\Lambda}$ anti-particles relative to the event plane angle Ψ_2 38
A.24 Number of produced Λ baryons relative to the event plane angle Ψ_2. 39
A.25 Number of produced K_s^0 mesons($yield$) relative to the event plane angle 40
A.26 Mean value of the invariant mass fitting for $\bar{\Lambda}$ 41
A.27 Mean value of the invariant mass fitting for Λ 42
A.28 Mean value of the invariant mass fitting for K_s^0 43
A.29 Sigma value of the invariant mass fitting for $\bar{\Lambda}$ 44
A.30 Sigma value of the invariant mass fitting for Λ 45
A.31 Sigma value of the invariant mass fitting for K_S^0 46

1 Introduction

"In order to assess the chances for creating a QGP in present or future relativistic heavy ion collision experiments, it is necessary to establish the collision dynamics and to prove the formation of a hot and dense initial "fireball" from the recent experiments"[1]

Kang Seog Lee , U. Heinz and E. Schnedermann

In relativistic nuclear collisions the goal of global data analysis, i.e. in terms of global observables, such as transverse energy and momentum or charged particle multiplicity (section §A.2), is to learn about the properties of nuclear matter under abnormal conditions. Pumping energy into a nuclear system is not consider enough, since a significant amount of compression is needed, that is large energy density values, something that is easily accessible in central collisions of high energy beams containing nuclei of equal size. Exploiting the *tomographic* study context that is offered by these collision systems, one is able to extract intriguing information on the behavior of nuclear matter, under extreme conditions of high temperature and great baryon density.

Probing the response of the hot and dense formed nuclear medium to these extreme conditions, labeled as the nuclear matter equation of state (EOS) in temperatures regions of $\sim 170 MeV$ and densities at least one order of magnitude greater than the normal nuclear density ($\approx 0.159 GeV/fm^3$) is of fundamental importance not only in Nuclear Physics and Field Theory, but constitutes also a basic prerequisite for regulating a series of astrophysical matters. Relativistic nuclear collisions under controlled conditions in the laboratories are a unique opportunity to study phenomena, such as the hadronization of matter and the impact on fragmentation in the former cases, while questions have already been addressed in the heavy ion research programs pertaining to the dynamics of the early universe during the first fractions of a second after the "Big Bang" or the evolution of neutron stars, crucial for the Astrophysics community. The experimental hints of the expected nuclear transitions are only derived form detection of the final products that are in normal state. Thus, one has to extrapolate from the end particles what happened during earlier stages, something that complicates also theoretical subsistence.

In the current report, observables which are relevant to the bulk properties of the deconfined hadronic matter have been incorporated, i.e. properties of the so-called QGP, nomenclature attributed to Edward Shuryak who was the first to examine the high temperature phase in detail in 1980[14]. More specifically, azimuthal distributions shapes of particles' transverse momentum p_T and invariant mass of three identified cases−neutral short Kaons K^0_s, Λ hyperons and $\bar{\Lambda}$ anti-baryons− through their charged daughter particles (section §A.4) have been investigated, in order that transverse collective flow, and in this case elliptic flow, to be detected, following up previous RHIC[15] and LHC[5] analyses.

In the early stage of the collision, that is before the interaction between the *fireball* constituents cease and hadrons freely stream to the detectors ($\tau \sim 20 fm/c \approx 10^{-22} sec$), dense and strongly interacting matter will lead to collective effects such as *transverse collective motion or flow*. An elliptic component of the former should be also present, on the grounds of the initial spatial anisotropy of the colliding system in non central cases (section §2). Most interestingly, this collective behavior has been proven to survive the hadronization process at RHIC energies[18], proposing a correlation between the observed amount of tranverse flow and the pre-hadronic stage state. This is considered as a signature for strong partonic interactions in the collision and an indication of a well developed and strongly interacting QGP (sQGP).

In the present analysis only the elliptic flow component of the overall anisotropic transverse flow has been considered, since the study context around the former has been designated in detail, thus it constitutes a method that could be adeptly manipulated in terms of the elementary character that a Bachelor's project bears. The script was organized in such a way that holds a noetic division in three main regions; in the first three sections (section §2−4) the theoretical and experimental instrumentation in which elliptic flow phenomena are dressed are presented, followed by the *Analysis* section (section §5.1 and 5.2) and then by the final *Results* (section §6) and *Discussion* (section §7) parts. The figures encapsulated in the text flow are only the ones that were considered essential for an uninterrupted reading, while the rest are given in the homonymous part (section §A.6). Finally, an Appendix has also been included, which provides the identification of the incorporated data sets, as well some additional, albeit crucial for a reader non affiliated with High-Energy terminology, elements.

[1] Referring to heavy ion experiments established in CERN SPS and Brookhaven AGS.

2 Elliptic Transverse Flow: Definition and Analysis Methods

"At a meeting in Jan'93, Jean-Yves[2] told me he was predicting in-plane elliptic flow at high beam energies. I responded that we had just discovered out-of-plane elliptic flow"

Art Poskanzer

From the very first experimental observables of collective emission patterns[38], the study of collective behavior that has been attributed to the constituents of the created matter and the interpretation of collective effects have attracted attention of both theoreticians and experimentalists. Progress has been made in both theoritical understanding of the relation between the collective tranverse flow components and internal medium processes, like thermalization or the creation of deconfined hadronic matter, and in the development of techniques suitable for flow investigations at high energies. Apart from being crucial in the theoretical instrumentation of the collision evolution, the importance to some extent of flow studies in other measurements, such as the determination of background contributions in particles' correlation analyses[39] or the most recent ones suggesting the local strong violation of parity and time-reversal symmetries[40], is also recognized.

Typically, in a heavy ion collision the region where the two nuclei overlap is not isotropic (figure 2.1 and A.4). The anisotropy of the medium-source will be largest immediately after the collision. As the system evolves, the spatial anisotropy is evened out and converted by multiple interactions into a momentum-space anisotropy. If particles free streamed from the formed area, their emission would be isotropic and the original spatial elliptic shape would never be transferred into momentum space. This collective behavior that reflects bulk medium properties plays a key role in the evolution of multiparticle production process.

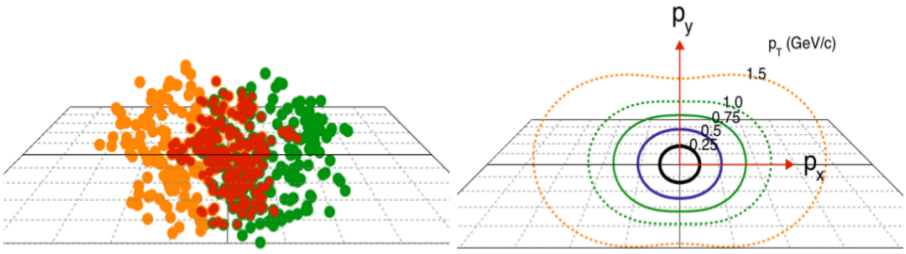

Figure 2.1: Transverse view of the initial overlap region marked with red(left panel- a Monte-Carlo simulation[17] of protons and neutrons in nuclei) and conversion from coordinate space into momentum space(right panel); the largest pressure gradient will be along the minor axis(bold line) of the elliptic overlap region, since as it is seen in the left panel the density in the short axis evolves most abruptly from the central maximum to minimum values at the edges. If pressure gradients are acting on the emitted particles, the former anisotropy will result in the elliptic anisotropy in the momentum space. The shape of the emitted particles' azimuthal transverse momentun distribution(see also figure 3.1) is shown for the indicated p_T values[16].

At high energies the longitudinal flow is well decoupled from transverse flow. Anisotropic transverse flow is used to be measured in a coordinate system transverse to the collision axis (figure A.4), due to the fact that at high energies the flow polar angles $\vartheta = \langle p_x \rangle / p \ll 1$ becomes very small, where $\langle p_x \rangle$ stands for the magnitude of the mean momentum along x-axis and p is the magnitude of the beam momentum. A convenient way for one to describe the azimuthal distributions is usually done by means of Fourier expansion, a technique that has been incorporated in the current analysis and is analytically described in section §3. Reference [22] by S.Voloshin, A.Poskanzer and R.Snellings provides an outline of the flow analysis methods that have been developed during time and incorporated in the different heavy ion experimental programs. The first STAR Collaboration outcome pertaining to the comparison of some flow methods using the same events and particle selection criteria *(cuts)* in order that validity to be ensured has been published in 2005. The results are shown in figure 2.2; one observes that fall into two distinct bands: those for two-particle correlations methods (upper band) and those for multiparticle methods (lower band). The difference has been attributed to the level of

[2] Referring to French physist Jean-Yves Ollitrault, who was the first to propose elliptic flow as a signature of hydrodynamic behavior[4].

dependence for the multiparticle methods case on nonflow effects, in which uncorrelated particles with the reaction plane do affect the magnitude of the calculated anisotropy parameters, and fluctuations, such as the initial spatial eccentricity fluctuations[21] (section §A.1).

Figure 2.2: Charged hadron v_2 (section §3) integrated over p_T and η as a function of centrality for the various methods indicated in the inset panel. *Standard* method(star) is the generalized method of the technique incorporated in this analysis. Blue-filled and open red circles stand for the cumulant method[19]. "True" flow values must be between these two bands[20].

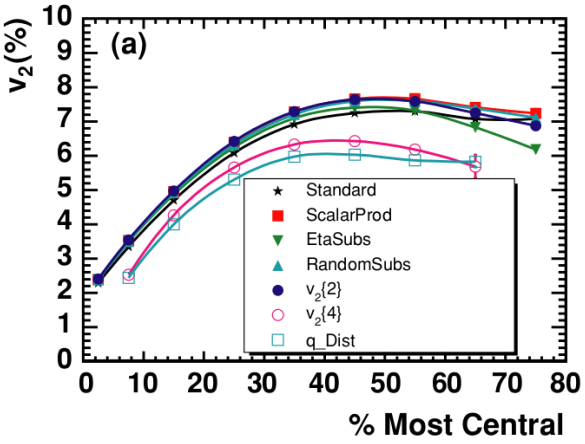

3 Fourier Expansion of Azimuthal Particle Distributions

"The study of flow in ultrarelativistic nuclear collisions has just begun and it is very important to define the subject and establish the terminology."

A.M.Poskanzer and S.A.Voloshin

In 1996 Voloshin and Zhang first proposed to decompose the azimuthal yield in Fourier moments[1], in order that to overcome a much model dependent method that had been used in CERN SPS and BNL AGS[2] previously. The essence of their proposed technique has been encapsulated by experimentalists later on, to develop a *standard* method for determining collision anisotropy parameters (section §4). The alternative approach that the formers introduced is to study the azimuthal event shapes obtained by the experimental data without having any model in mind. In this case one investigates the shapes of azimuthal distributions in the general direction of detecting and comprehending anisotropies of different kinds. To get more detail in the extracting and comprehending of the event shapes, it is vital first to provide with the theoretical instrumentation, as was originally proposed by its originators.

The particle azimuthal distributions can be constructed based on quantities such as transverse momentum, multiplicity, or transverse energy in relatively narrow pseudorapidity windows. Let us denote with r(ϕ) the azimuthal distribution function of the respective quantity which is under study[3], that is $\frac{dN}{d\phi}$ where N stands for the total number of charged particles emitted at a specific azimuthal angle $\phi = \phi_{lab} - \Psi_{RP}$ (section §A.2). The function r(ϕ) can be then constructed from the experimental data and be explicitly written in the form of Fourier expansion as:

$$r(\phi) = \frac{x_0}{2\pi} + \frac{1}{\pi}\sum_{n=1}^{\infty}[x_n cos(n\phi) + y_n sin(n\phi)] \tag{3.1}$$

The coefficients x_n and y_n (zero order included) in the above Fourier expansion are integrals of r(ϕ). Let us assume that the reaction plane lies in x-axis of the initial spatial geometry. The integrals become sums over particles for the case of a finite number of particles:

[3] The angular part is an element of the invariant cross section which could be described in terms of experimental observables $E\frac{d^3N}{p_T dp_T dy d\phi}$.

$$x_n = \int_0^{2\pi} r(\phi)cos(n\phi)d\phi = \sum_i r_i cos(n\phi_i) \tag{3.2}$$

$$y_n = \int_0^{2\pi} r(\phi)sin(n\phi)d\phi = \sum_i r_i sin(n\phi_i) \tag{3.3}$$

where i runs over particles produced in the respective rapidity window, and $\phi_i \equiv \phi_{lab(i)}$ is the azimuthal angle of the ith particle. Each non zero x_n and y_n pair give the value of non zero component of the corresponding harmonic coefficient, which is defined as

$$\upsilon_n = \sqrt{x_n^2 + y_n^2} \tag{3.4}$$

The main advantage of the Fourier expansion is that the results can be directly compared to the theoretical predictions for which the reaction plane has been taken to be the plane containing the theoretical impact parameter (section §A.1) or most importantly to simulations unfiltered for the detector acceptance! The limitation on the other hand is that there should be sufficient number of particles in each window. Thus, a series of corrections have been used in the analysis of flow phenomena, such as applying weights to the particles (the r_i factors in (3.2) and (3.3)) or constructing azimuthal functions for certain types of particles separately.

Last, but not least, a unique feature of this approach is the correlation of flow effects between different types, on the grounds that the Fourier coefficients in (4.4) corresponding to different harmonics bear a clear physical meaning. In figure 3.2 a simulation that incorporates the correlation up to the fifth anisotropy parameter υ_5 is presented. Without any flow the function r(ϕ) is constant, since all Fourier coefficients except x_0 are zero. On the contrary, if flow exists, r(ϕ) is no longer constant and, with r(ϕ) being the transverse momentum distribution for instance (let us denote with r'(ϕ)), the shape of the azimuthal distribution is no longer a circle centered at zero point of the transverse plane (figure 3.1). In general the appearance of transverse anisotropic flow in nuclear collisions is expected from a non-zero value of impact parameter.

Then the first order harmonic coefficients x_1 and y_1 correspond to an overall shift of the distribution in the transverse plane; such flow is called *directed* flow. More specifically, as it is easily seen from (3.2) and (3.3), x_1 and y_1 are X and Y components respectively of the total transverse momentum of the particles produced in a specified rapidity window, while υ_1 is the magnitude of the total sum vector (*flow vector*) of particles transverse momenta. The direction of flow due to symmetry is to coincide with the reaction plane angle $\Psi_1 = \Psi_{RP}$ (repulsive flow), or point in the opposite direction $\Psi_1 = \Psi_{RP} + \pi$ (attractive flow). This is the reason why the first harmonic is labeled as *directed*, since such a flow has a specific direction.

The non-zero second harmonic[4] describes the eccentricity of an ellipse-like distribution. If one approximates the distribution by an ellipse, then the second coefficient υ_2 has a direct correlation to the magnitude of the eccentricity and equals to the difference between the major and the minor axis (the two dashed lines perpendicular to each other in figure 3.1). The latter gives rise to both negative and positive values of the elliptic flow parameter. The orientation of major axis Ψ_2 can be only in the direction of Ψ_{RP} (positive υ_2) or $\Psi_{RP} + \frac{\pi}{2}$ (negative υ_2). In the first case, the major axis points into the reaction plane, while $\Psi_2 = \Psi_{RP} + \frac{\pi}{2}$ indicates that the orientation of the ellipse is perpendicular to the reaction plane, which is the case for squeeze-out flow, one of the very first components of the collective flow that has been observed since 1989[13].

[4] For an analysis of higher than the second harmonics the author refers to page 5 in [1].

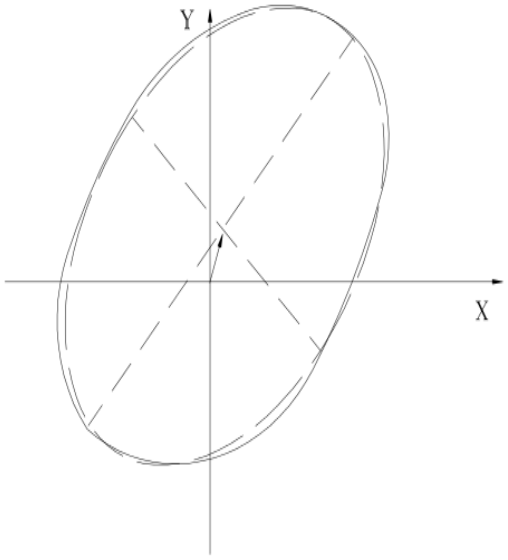

Figure 3.1: A schematic of an ellipse-like distribution–the elliptic flow component is modulated by harmonics of different order– in polar coordinates (X,Y) where $X \equiv p_x$ and $Y \equiv p_y$; if flow exists, r'(φ) is no longer constant.

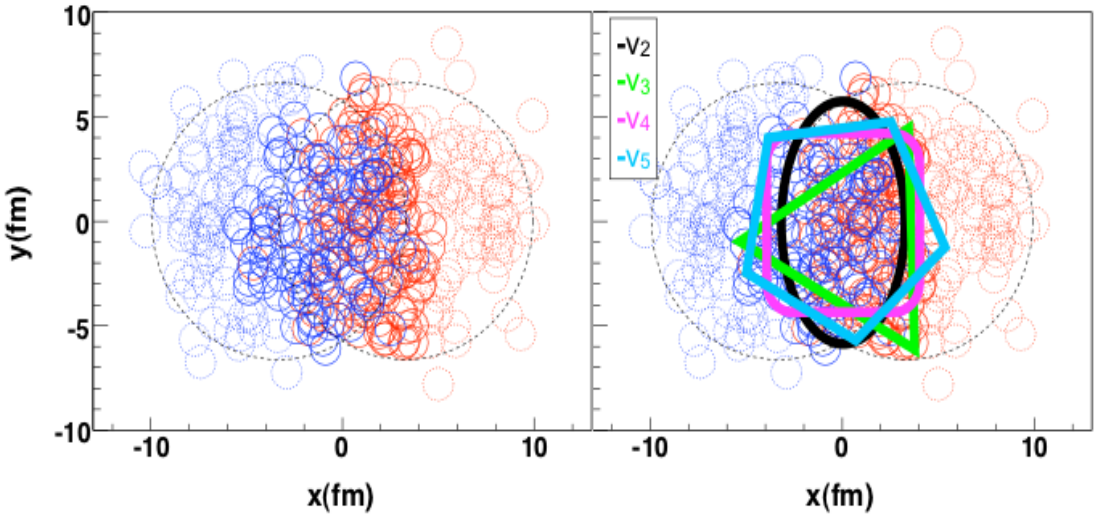

Figure 3.2: Two identical plots from a simulated Pb-Pb collision at $\sqrt{s_{NN}} = 2.76TeV$ with the PHOBOS Monte Carlo Clauber[3]. In the right panel shapes laid on top to visualize different flow moments.

4 Reaction Plane Estimation– The Event Plane Method

Based on their definitions (3.4), the calculation of v_n coefficients goes through the experimental determination of the reaction plane. This is achieved by the estimation of the reaction plane angle, an approximation that as mentioned in the previous section leads to the *event* plane. Thus, the Fourier expansion is evaluated with respect to the latter and, due to the finite number of the detected particles, a limitation is raised on the *event* plane resolution, that is the accuracy with which the reaction plane orientation is determined.

In this analysis the second order *event* plane is determined from the data on an event by event basis, according to the formula proposed by A. Poskanzer and S.Voloshin[24]

$$\Psi_n = \frac{1}{n} tan^{-1}\left(\frac{\sum_i r_i sin(n\phi_i)}{\sum_i r_i cos(n\phi_i)}\right) \tag{4.1}$$

which is derived combining (3.2), (3.3) and

$$x_n = \upsilon_n cos(n\Psi_n) \tag{4.2}$$

$$y_n = \upsilon_n sin(n\Psi_n) \tag{4.3}$$

Due to the spatial reflection symmetry with respect to the *event* plane $\phi \leftrightarrow -\phi$ the sine terms vanish in (3.1), so r(ϕ) can be finally written with respect to the nth order *event* plane as

$$r(\phi) = \frac{1}{2\pi}\left(1 + \sum_{n=1}^{\infty} 2\upsilon_n cos\left[n\left(\phi_{lab} - \Psi_n\right)\right]\right) \tag{4.4}$$

With a perfect detector the azimuthal distribution of the event plane would be isotropic, although limitations due to the limited coverage and the imperfect efficiency of a real detector lead to biases, something that can be removed by applying correction methods, so as to the distribution of *event* planes to be isotropic and consequently the determination of the υ_n coefficients to be more accurate. All these corrections contribute to a better reaction plane resolution, although in the current analysis such a correction procedure has not been implemented, thus no correction factors r_i are present in (4.1). The υ_n coefficients that are present in (4.4) are p_T and η (section §A.2) functions, so are distinguished by their integrated values that were examined in the previous section. During the analysis, since only differential values have been taken into consideration, **the υ_2 notation corresponds to $\upsilon_2(p_T)$ dependence,** apart from the *Discussion* section where discrete reference has been done.

5 Analysis

5.1 Extracting the Reaction Plane and Elliptic Flow of Charged Particles

All the software is written in C++ within the ROOT analysis framework [12]. A simple source code that incorporates the Fourier decomposition in terms of the second harmonic only[5] has been used. Before proceeding one should examine if the response of the *event* plane method is reasonable. Indeed, having been extracted based on 4.1 using the azimuthal transverse momentum distribution of primary tracks in the $0.5 < p_T < 3GeV/c$ region, the reconstruction of the reaction plane seems to be in good agreement with what it is expected by construction, that is a smooth and flat distribution. The small observed fluctuations account for the small number of total events that were encapsulated due to technical limitations in the computer storage memory. A reconstructed reaction plane in 20-40% centrality with a significant larger statistical sample is presented in figure A.11. The choice for non implementation of weighting factors is also attested by the ATLAS publication[5], whose results have found to be insensitive to the weighting within the systematic uncertainties. In figure A.10 the reconstructed reaction planes for the (0-80)% centrality regions are presented.

After having secured that the event plane method works properly, one has to calculate the correlation of individual track azimuthal angles with the reconstructed reaction plane and verify that physical ATLAS results are reproduced. This could be done by constructing the azimuthal distribution with respect to the *event* plane of transverse momentum for instance including all the identified charged particles, which is translated in the programming language as a two dimensional p_T vs $(\varphi_{lab} - \Psi_2)$ histogram in each specified centrality region(figure A.12). Doing so, the next step that rationally follows in order to deduct the value of the second coefficient υ_2, is to extract the shape of the above distribution for every p_T bin. By choosing a relatively small step (0.5GeV/c) to scan the whole p_T region and inserting the fit curve

$$f_1(x) = 1 + 2\upsilon_2 cos(2x) \tag{5.1}$$

for arbitrary x values[6] one gets plots like the ones presented in figure A.13–figure A.15, which are the 0.5GeV/c pace projections of the p_T vs $(\varphi_{lab} - \Psi_2)$ histogram on the y-axis. There is a clear sinusoidal modulation for all centralities and transverse momentum regions, apart from the most peripheral events in the high p_T bin (the bottom panels in figure A.15) due to the low particle multiplicity that characterizes

[5] From now on all elements inserted in the analysis refer to the second harmonic parameter. For example the *event* plane refers to the second order (reconstructed) reaction plane.

[6] The quantity x=$\varphi_{lab} - \Psi_n$ has a minimum periodicity of 2π/n, so that for the $n = 2$ case equals to π rad.

these regions. This modulation is largest in the 20-60% centrality region, and weakens for the more central and peripheral events. One may observe that the fitting distribution is normalized to unity, in order to get rid of a second parameter in 5.1 and to simplify the extracting of v_2 values, which are then taken simply by

$$v_2 = \frac{f_{1,max}(x_o) - 1}{2} \tag{5.2}$$

since for those x_o that f_1 is maximized the cosine factor gets to unity. The Fourier harmonic coefficient ends up to be correlated with the information of how well or not the azimuthal distribution follows a perfect $1 + cos(2\phi)$ modulation.

Once anisotropy parameter values have been determined, one has to plot the elliptic flow parameter v_2 against p_T in each centrality interval specified above. The results presented in figure A.16 are also compared to the ATLAS same pseudorapidity region experimental results of the elliptic flow of charged particles in Pb-Pb collisions at $\sqrt{s_{NN}}$ =2.76TeV. In general terms, there is quite a good agreement between them, following the pattern of a rapid rise up to p_T ≈3GeV/c, a decrease out to 6-7 GeV/c and then a weak variation dependence beyond 9-10GeV/c with relatively large statistical uncertainties.

The same trends could also be seen for the $1 \leq |\eta| \leq 2$ and $2 \leq |\eta| \leq 2.5$ regions in the ATLAS experiment. This centrality pattern at LHC energies, where hydro-dynamical type of the system evolution−creation of regions of QGP− is predominant, is easy to follow. In this great energy and parton density regime interpretation of elliptic flow centrality dependence is mainly based on collision geometry. The more central a collision is, the greater number of particles are being produced in more symmetrical spatial region. Thus, in mid-centrality intervals, where the colliding nuclei form a non symmetric overlapping region, in which *fireball* constituents could be thermalized, there is an asymmetry transition to momentum space, something that leads to the increase of the measured asymmetry parameter v_2. In the most peripheral collisions v_2 behavior is non trivial though and in general is expected to be lowered, due to the degraded eccentricity of the initial collision shape that characterizes such collisions(see also section §7). This trend seems not to be clearly reproduced by experimental outcomes[37].

5.2 Anisotropy parameter $v_2(p_T)$ for K^0_s, Λ and $\bar{\Lambda}$; mass *splitting* and quark scaling

The azimuthal distributions with respect to the extracted *event* plane of the invariant masses have been used for the extracting of the anisotropy parameters v_2. This is done by constructing invariant mass distributions $\Delta m - (\phi_{lab} - \Psi_2)$ (figure A.17−A.19) for those tracks that have been identified to be the charged decays (figure A.9) of each one neutral particle under study, that is K^0_s, Λ and $\bar{\Lambda}$. In figure 5.1 invariant mass distributions $\Delta m - (\phi_{lab} - \Psi_2)$ within the $3.5 \leq p_T < 4.5$GeV/c region are shown in a more descriptive way, in which the elliptic flow sinusoidal pattern is evident. The term *invariant mass* is used rather naively and refers to the difference between the mass of the reconstructed particle alleged to be a V^0 and the mass extracted by indices.

Interestingly, ALICE data allow to include transverse momentum bins not possible to be incorporated in RHIC analyses of the past years due to large statistical fluctuations. In the current analysis, transverse momentum up to 8.5GeV/c for K^0_s mesons, and up to 7.5GeV/c for Λ baryons and their $\overline{\Lambda}$ anti-particles has been considered, signature of the outstanding progress done concerning accelerating and detecting facilities in the High-Energy Physics field. At variance, low p_T bins in the 0.5-1.5GeV/c region, have been excluded on the grounds of the large background to signal ratio that characterizes these regions; by subtracting background contributions, it is possible relatively low p_T bins to be also included, albeit this subtraction procedure has not been considered as one of the primary goals of the current analysis.

Then, one has to project on the horizontal axis, while scanning the $\phi_{lab} - \Psi_2$ region. The invariant mass distributions based on the Breit-Wigner formula[24] are characterized by Gaussian-like distributions with their peaks centered at zero for this case. Since background contributions are present, the fitting process involves a polynomial superposition at the basis of the distributions, thus the fitting in the executable file bears the general form:

$$f_2 = [0] \cdot \frac{exp(-0.5 \cdot ((x - [1])/[2])^2}{(\sqrt{2\pi}) \cdot [2])} + pol2[3] \tag{5.3}$$

The arithmetic values inside the square brackets stand for the Gaussian fitting parameters, that is [0] corresponds to the number of produced particles for which the fitting has been implemented (*yield*), [1] constitutes

the mean value which in this case should be around zero, while [2] is the sigma parameter and correlates to the width of the *bell*. The second term on the right side in (5.3) represents a second degree polynomial and the [3] notation is a programming convention which accounts for the total enumeration of the using parameters, namely the enumeration for the *pol2* function begins with the parameter classified as third in the overall fitting function.

In general terms, the procedure that one follows in order for the fitting to be characterized with the minimum deviation from the experimental points, is first to choose such Gaussian parameters to ensure that its correspondence is reasonable. After having extracted the *bell's* parameters, the background fitting is usually done in steps, that is in ascending level in terms of the polynomial degree; first adding a zero degree polynomial (a constant) and gradually climbing in order up to a degree that the parameterization behaves most prominently.

The transverse momentum bins have been selected in a way that their distance to be 1GeV/c. Thus, for each p_T bin−seven in total for K^0_s and six for Λ and $\bar{\Lambda}$ respectively− there are twenty invariant mass distributions (figure A.20−A.22), so as to the whole $\phi - \Psi_2$ area − $(-\frac{\pi}{2}, \frac{3\pi}{2})rad$ − to be fully scanned and the angular pace is automatically adjusted by the ROOT context. After having secured that the fitting responded reasonably for all angular bins inside a given p_T bin, which is done merely by examining the flat distribution of the mean (figure A.26−A.28) and sigma (figure A.29−A.31) parameters, one has to verify that the *yield* follows a sinusoidal pattern by inserting an alike to the (5.1) modulation:

$$f_3 = N_{mean}\left\{1 + 2v_2 cos\left[2\left(\phi - \Psi_2\right)\right]\right\} \tag{5.4}$$

where N_{mean} is the mean number of the produced particles under consideration in the respective p_T bin. The results of the fitting distribution are shown in figure A.23−A.25 and the extracted v_2 values as a function of transverse momentum for all three cases are presented in figure 5.2. Finally, the v_2 vs p_T correlations have been scaled with the number of the constituent quarks (figure 5.3).

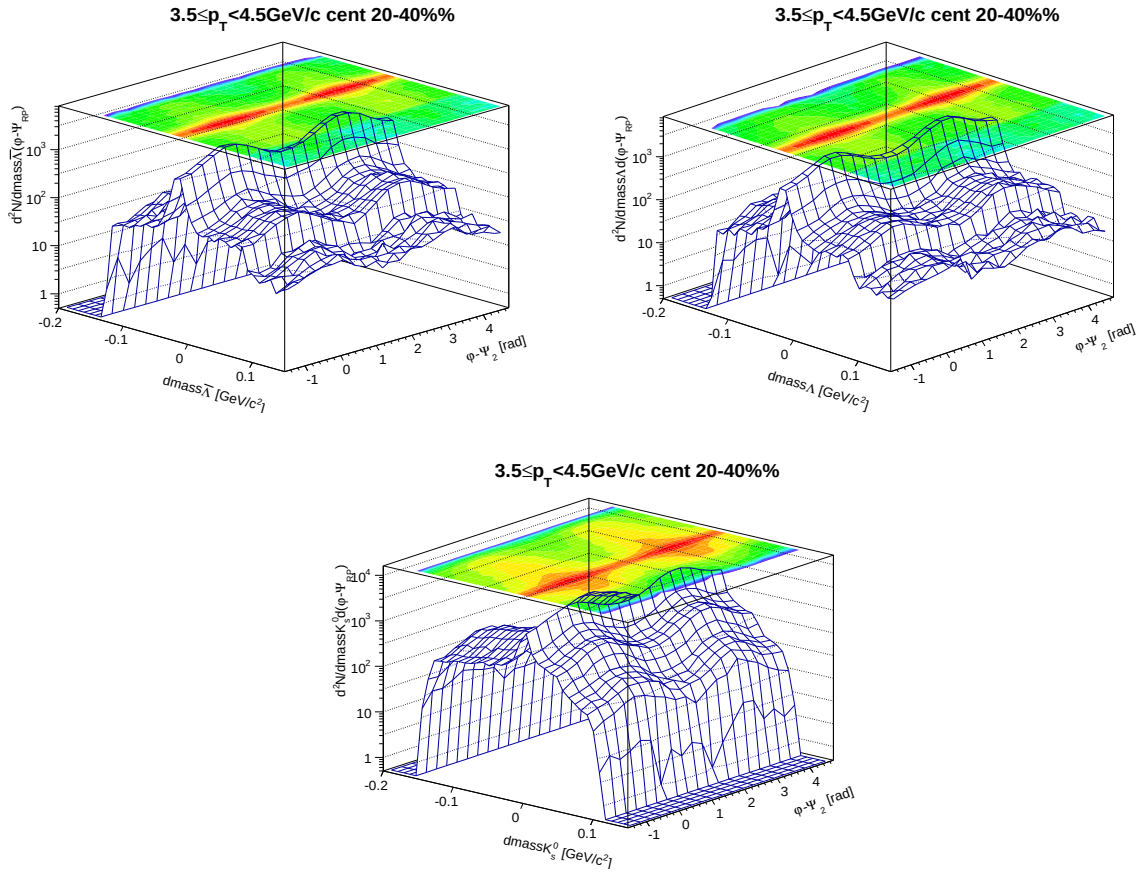

Figure 5.1: Invariant mass distributions $\Delta m - (\phi_{lab} - \Psi_2)$ for $\bar{\Lambda}$, Λ and K^0_s; elliptic flow pattern is evident also for the background, i.e. particles with masses relative to ones of the three above cases ($\Delta m \rightarrow 0$ GeV/c^2). The contour views (figure A.13-A.15) are also drawn on the top.

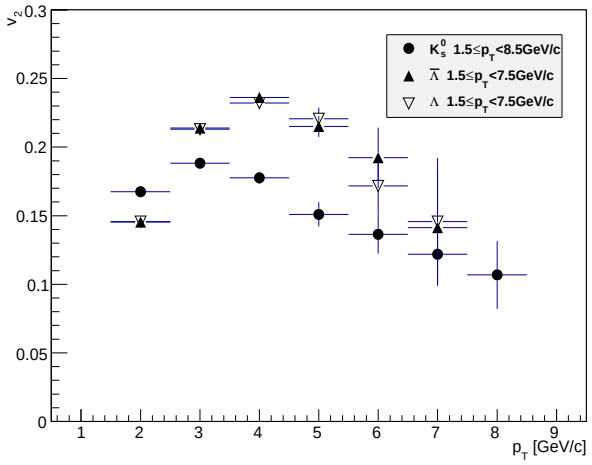

Figure 5.2: Anisotropy parameter v_2 as a function of transverse momentum for K^0_s (filled circle), Λ (open triangle down) and $\bar{\Lambda}$ (filled triangle up) for the indicated in the inserted panel p_T regions.

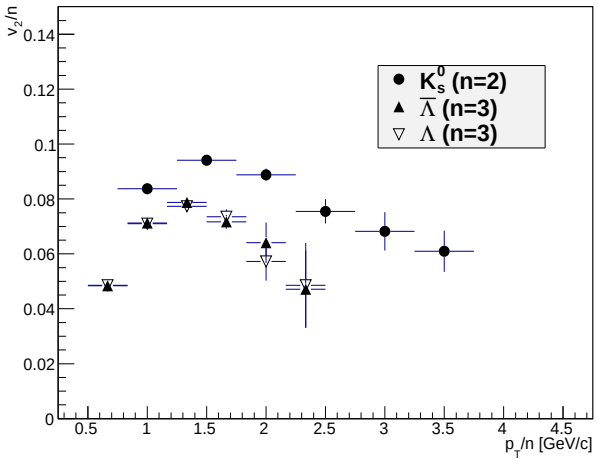

Figure 5.3: Anisotropy parameter $\upsilon_2(p_T/n)$ as a function of p_T/n for K^0_s (filled circle),Λ (open triangle down) and $\bar{\Lambda}$ (filled triangle up) for the indicated in the inserted panel n values. The $7.5 \leq p_T < 8.5$GeV/c interval for the K^0_s has been skipped.

6 Results

In this analysis, the dependence of the second order anisotropy parameter υ_2 on transverse momentum for eight 10% centrality intervals and for tracks within $|\eta| < 0.8$ region was examined. The non monotonic pattern, which is common for all centrality intervals, follows a rapid increase up to $p_T \approx 3$GeV/c giving its maximum value 0.26 in 70-80% centrality interval, a decrease out to 6-7GeV/c and then a weak variation with large statistical uncertainties. The extraction of υ_2 values on the grounds of the large particle multiplicity were done by firstly constructing the double differential $\frac{d^2N}{dp_T d(\phi_{lab}-\Psi_2)}$ distribution and then applying the Fourier decomposition (3.1) for transverse momentum bins up to 20GeV/c. This technique has partially included the *standard* method proposed in Ref. [23], by means of determining the second order *event* plane angle Ψ_2 based on the azimuthal momentum distribution of primary tracks in the $0.5 < p_T < 3$GeV/c region. The transverse distribution of the former (figure A.10-A.11) was found to be flat, consistent with what is expected by its construction, accounting for the isotropic azimuthal coverage of the detector and certifying its fine responce.

At variance with the selection of the azimuthal transverse momentum above, the evaluation of the υ_2 parameters for the identifying cases of K^0_s, Λ and $\bar{\Lambda}$ were done considering the invariant mass azimuthal distributions. ALICE data allow to proceed much further than it was feasible at RHIC energies over the past years, mainly in terms of p_T bins. The υ_2 dependence on p_T up to 8.5GeV/c for the K^0_s, and up to 7.5GeV/c for the Λ and $\bar{\Lambda}$ is presented in figure 5.2. In the K^0_s case υ_2 gets its maximum value ~ 0.17 at around 3GeV/c, while for the other two cases peak values ~ 0.21 are observed at slight greater p_T, that is about 4GeV/c. For still larger p_T, υ_2 is gradually declined for all three cases. Scaling with the number of constituents quarks is finally examined. In figure 5.3 both axes are scaled by two or three corresponding either to meson or baryon (anti-baryon) case respectively. The outcome is in clear disagreement with what is expected by the well established at RHIC energies quark scaling, that is the three distributions to top on each other.

7 Discussion

In heavy ion collisions, the particle azimuthal distribution measured with respect to the reconstructed reaction plane is not isotropic and the magnitude of this anisotropy is characterized by Fourier components. The $v_n(p_T)$ coefficients present in (3.1) were thought to be p_T and η function, thus they are labeled under *differential* flow, while *integrated* flow stands for the average over the above correlation variable regions. However, experimental evidence at LHC pertaining to the weak dependence on η, at clear variance with PHOBOS experiment[25] at $\sqrt{s_{NN}} = 200$GeV/c, suggests even flat η dependence. As a result, only p_T correlation has been taken under consideration in the current analysis.

The non monotonic dependence is well established in all centrality intervals, albeit a key difference is that the $v_2(p_T)$ peak values, that is those around $p_T \approx$3GeV/c, seem to follow an increasing trend with increasing centrality, getting its maximum 0.26 in the (70-80)% centrality interval, 62.5% higher than the respective in the same centrality interval ATLAS value. In general terms, at heavy ions experiments of lower energies the centrality dependence was believed a combination of contradictory trends arising from elliptic flow origins, mainly by means of rescattering among the system's constituents that is driven by the collective motion, and spatial eccentricity of the collision zone. The amount of rescattering is expected to increase with increasing centrality, while the eccentricity declines. For a detailed discussion author refers to [42].

However, the extracted values in (60-80)% region could not be considered dependable by means of auto-correlations that are less scarce in increasing centrality intervals due to the low particle multiplicity. It has been found[36] already from 1985 that there is a trivial correlation between the particle's azimuthal angle with respect to the angle of the reconstructed reaction plane in case that same particles are being used in determination of both anisotropy parameters and reaction plane angle. Thus, auto-correlations have to be removed, meaning in practice that particles which have been used in defining the *event* plane should be removed, if necessary. In current analysis for instance one should keep track of the particles in $0.5 < p < 3$GeV/c. The comparison with the more sophisticated ATLAS measurement provides constraints that above (50-60)% region our method response is biased, which is reflected in the abrupt decrease in $v_2(p_T)$ values around $p_T \approx$3 GeV/c (bottom panels in figure A.16).

The conversion of the initial spatial anisotropy into momentum space due to multiparticle processes that happen inside the hot and dense formed region is quantified primarily by the $v_2(p_T)$ magnitude that corresponds to an elliptic component of the overall transverse collective flow. While mathematically correlated to the geometric anisotropy characteristics of the overlapping region through eccentricity terms, $v_2(p_T)$ carries also information about the number of the emitted particles in a specific direction; based on (5.1) the ratio of particles emitted in the direction of the *event* plane (in-plane) to those perpendicular to it (out-of-plane) is given by $\frac{1+2v_2}{1-2v_2} \sim (1+2v_2)^2 \sim 1+4v_2$. Thus for the maximum obtained value ∼0.26 the latter produces a value around 2 for particles emitted with $p_T \approx 3$GeV/c.

This remarkable deviation from expectations of free-streaming hadrons is a signature that collective behavior during the different evolution stages survives hadronization and the system maintains a memory of its original geometry. To be mentioned that remains an open question if collective flow is present in all evolution stages, albeit already from its first observation at RHIC[30] the presence of elliptic flow was taken as a signature of the rapid thermalization that follows the initial formation of the system.

Overall, the image of the differential $v_2(p_T)$ has not been yet explained in terms of a punctual global theoretical context, except from low $p_T < 2$ GeV/c region[28], where hydrodynamical models assume local thermal equilibrium at the early stage of formation of the system, followed by an evolution characterized by an EOS. This successful hydrodynamic description of the $v_2(p_T)$ data in the above momentum range fed RHIC physicists' belief on a perfect liquid matter state[32]. The saturation that seems to accompany $p_T >$ 6-7GeV/c regions could be attributed to the energy loss asymmetry of the jet-quenching process[26] that is expected to dominate this p_T region, according to which partons propagating the medium loss great amount of energy mainly due to radiation (gluon bremsstrahlung) leading to highly suppressed hadrons in terms of momentum after fragmentation. In the same article, according to a second scenario, this saturation could be treated as a consequence of the transition from soft to hard production processes occurring for pions and protons at different p_T areas.

At RHIC energies there was mounting evidence[20] that in a dense phase-space scenario, colored partons are strongly affected by the existence of neighboring partons and essentially coalesce into colorless bound states, much like the fusion process in the formation of light nuclei in stellar environments. As the system of deconfined quarks cools during its expansion, pairs and triplets of quarks neighboring phase-space coalesce to become the valence(constituents) quarks of mesons and baryons respectively. Then, the azimuthal anisotropy parameter $v_2(p_T)$ of a bulk system of quarks and the hadrons that the former coalesce are related under

circumstances by [27]

$$v_2^h(p_T) = \sum v_2^q(x_q p_T) \tag{7.1}$$

where q stands for a quark−or anti-quark referring to the meson case− that carries a fraction x_q of the sum of the final hadron momentum. Supposing that the constituents quarks have similar azimuthal distributions, that is $v_2(p_T)$ values that approximate each other, (7.1) produces the scaling pattern observed at RHIC

$$v_2^h(p_T) = n v_2^q(p_T/n) \tag{7.2}$$

where n is the number of constituents quarks for the meson or baryon (anti-baryon) cases. The above relation could be reformed in order that its significance be more apparent:

$$\frac{v_2^B(p_T/3)}{3} = \frac{v_2^M(p_T/2)}{2} \tag{7.3}$$

However, this is in direct disagreement with the results shown in figure 5.2. There is a clear sign of elliptic flow scaling violation pertaining to strange particles. Moreover, there is experimental evidence at LHC[43] that this violation holds also for both protons and pions, thus it is not restricted to strange flavor and major concern on coalescence as a process of hadron production in intermediate and low p_T is like to be raising. In the next several years, heavy ion programs are going to play a key role in extrapolating informations relating to hadronization procedure(s) in an overall image incorporating promising candidates standing for the coupling between the medium and the jets. An extensive effort to encapsulate quark coalescence models and their limitations was made in [27].

Interestingly, hydrodynamics models unmask some features concerning the $v_2(p_T)$ mass dependence in the low momentum region; heavier particles have lower $v_2(p_T)$ (figure 5.3). This mass ordering might account for a boosted thermal model, as it was examined for instance in the RHIC preliminary Ref.[33]. As the particles are shifted towards higher p_T, the momentum space for lower p_T becomes depopulated, which is translated to an overall degraded $v_2(p_T)$ magnitude at a given $p_T < 3$GeV/c value, since this depopulation holds most for the in-plane direction. For the heavier particles case they should receive on the grounds of the collective motion a larger p_T kick, which is then reflected to the measured $v_2(p_T)$ values, reduced relative to ones corresponding to lighter particles. At higher p_T, the mass ordering is broken with more massive baryons to exhibit larger $v_2(p_T)$ values than mesons. This behavior is proven to be non trivial, since hydrodynamical calculations fail to reproduce it. The author refers to the respective *Discussion* section in [15], where comparing with other models is also made and some primary conclusions are drawn. Finally, there is evidence that baryon $v_2(p_T)$ to be almost equals to anti-baryon $v_2(p_T)$ up to 4.5GeV/c, in contradiction with previous RHIC analysis[31] and then again a non trivial interrelation.

8 Acknowledgements

The author expresses his gratitude on the feedback and support that has received by the ALICE members during the 2012 spring semester at Lund University; author's supervisor Peter Christiansen provided crucial support in the direction of software analysis and the overall structure of the thesis. As for the rest of the research group, Anders Oskarsson played a decisive role in choosing heavy ion field as the general topic of the project with his inspiring words, Evert Stenlund in supervising a literature project on jet quenching as part of a master course, the post-doc Antonio Ortiz Velasquez in both writing the first part of the code for reading the data and explaining the major criteria selection procedure that is implemented in ALICE detector, the two current ALICE Ph.D. students, Martin and Tuva whose experimental work constitutes admiring examples of great effort and perseverance, and finally my friend and master student Puria in sharing nice conversations pertaining to the first analysis' part which has been done in common.

Finally, Carl Erik Magnusson contributed most to the final thesis version, providing essential feedback on grammatical, linguistic and textual issues of the script.

A APPENDIX

When observed from the centre of mass (CM) frame, two nuclei accelerated to highly relativistic speeds will appear as two flat pancakes due to Lorentz contraction(figure A.1). The radius of a nuclei is approximately given by $R \approx 1.2 \cdot A^{1/3}$, where A stands for the atomic mass number. For the Pb case this produces a value around 7 fm (1 fm $=10^{-15}$m). The system after a collision is shown in figure A.2; the particles inside the overlap region, known as participant particles, create a *fireball*, which is described by local thermal equilibration and collective expansion. The particles outside of the overlap area continues along their original trajectories, and are labeled as spectators. At the high achieved LHC energies, the latter do not have time to interact with the other particles, since carry so much momentum.

For the Appendices (A.1) and (A.3) author consulted Ref. [15] and [41].

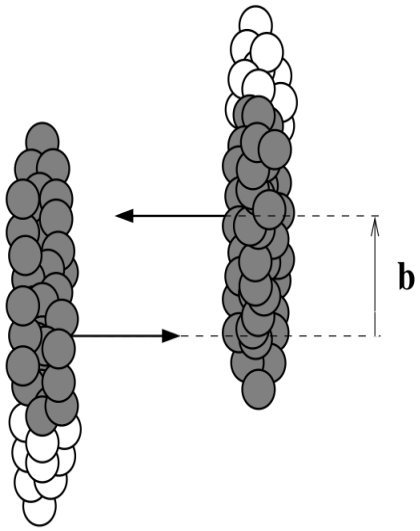

Figure A.1: A heavy ion collision seen from the (CM) frame.

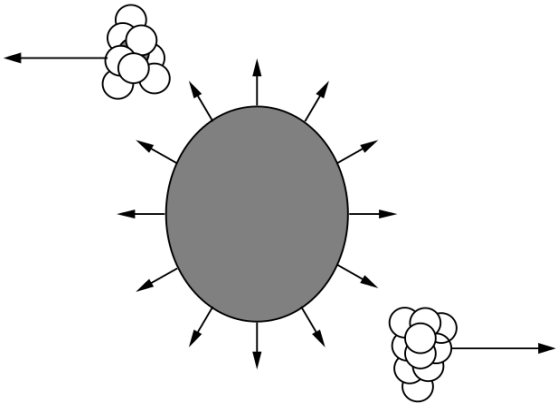

Figure A.2: Spectators and participants; at lower energies the spectators has a shadowing effect on particles in the fireball[6].

A.1 Collision Geometry and Source Eccentricity

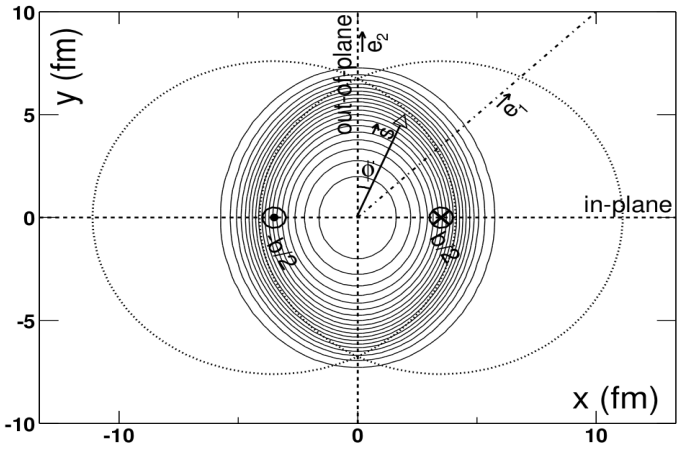

Figure A.3: Coordinate system for the transverse plane in heavy ion collisions. Contours of the overlap density are also presented. Azimuthal angle $\phi' = \phi - \frac{\pi}{2}$ meausred with respect to the y-axis is shown, where the reaction plane is aligned with the x-axis. $\vec{e}_1$ and $\vec{e}_2$(y-axis) are generalized coordinates used in an analytic calculation of the fourth-harmonic eccentricity[15].

In figure A.3 the coordinates in the azimuthal plane of the collisions are presented. At the LHC, the coordinate system is such that the z-axis is parallel to the collision axis (in or out of the page as indicated by the $\otimes$ or $\odot$ respectively in figure A.3), the x-axis is horizontal, pointing into the centre of the accelerator and the y-axis is vertical, pointing up. The nominal interaction point (IP) is at the $(0,0,0)$ −coordinate; the beams are aimed such that collisions take place around this point, since directions of the colliding beams do not coincide always with the collision axis. Thus the collision point also has to be measured, which is called the *primary vertex* or sometimes just *vertex*(section §A.3). The distance between the centers of the colliding nuclei is given by the magnitude of the impact parameter vector $\vec{b}$, which lies in a plane perpendicular to the collision axis and contains the two centers(figure A.4).

In the extraction process of v_2 values (section §5.1) , ϕ was defined with respect to the reaction plane, that is the plane spanned by $\vec{b}$ and the beam direction, albeit in the eccentricity calculation models, $\phi' = \phi - \frac{\pi}{2}$ is defined with respect to the y-axis, so as to v_2 and the 2nd-harmonic eccentricity, which generates the elliptic flow, have the same sign. In this way, due to this relation between the initial spatial anisotropy and the elliptic flow, it is more convenient to estimate the fluctuations in $v_2 \propto \epsilon_2$ that stem from the eccentricity of second order ϵ_2.

The definition of the second order eccentricity which generates the elliptic flow is

$$\epsilon_2 \equiv \langle y^2 - x^2 \rangle / \langle y^2 + x^2 \rangle \tag{A.1}$$

where the angular brackets denote an average over all particles. The ϵ_2 values are taken from model calculations (see [21] for instance). Calculation on eccentricity fluctuations are important for multiparticle elliptic flow methods, thus estimation of what the possible effect of spatial eccentricity fluctuations might have on determining v_2 magnitudes is crucial.

A.2 Kinematic Variables

The azimuthal components of a particles momentum $\vec{p}_x$ and $\vec{p}_y$ are used to define its transverse momentum

$$p_T \equiv \sqrt{p_x^2 + p_y^2} \tag{A.2}$$

The transverse mass/energy of a particle having mass m_0 is

$$m_T \equiv \sqrt{p_T^2 + m_0^2} \tag{A.3}$$

so that the transverse kinetic energy of the particle is $m_T - m_0$. The transverse kinetic energy is often used in place of p_T. In the laboratory frame, the azimuthal angle of a particles momentum is simply

$\phi_{lab} = tan^{-1}\left(\frac{p_y}{p_x}\right)$. When the reaction plane can be measured with infinite accuracy the azimuthal angle can be measured with respect to the azimuthal angle of the reaction plane Ψ_{RP} :

$$\phi = \phi_{lab} - \Psi_{RP} \tag{A.4}$$

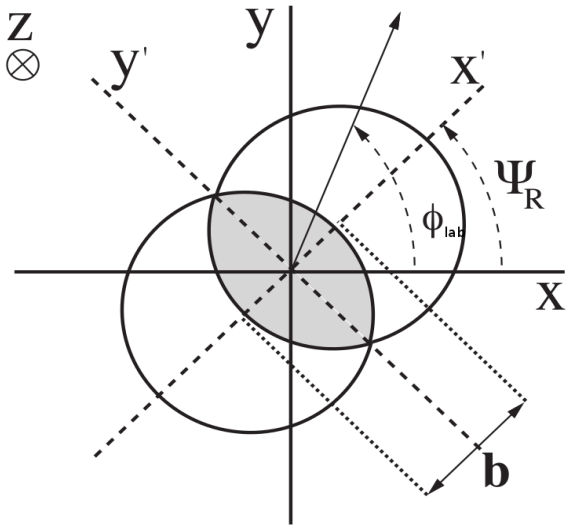

Figure A.4: Schematic view of a non-central nucleus-nucleus collision in the transverse plane. Ψ_{RP} denotes the reaction plane angle and (x', y') is the flow coordinate system.

In parallel to the transverse coordinates, the natural velocity(*rapidity*) in special relativity is used as a longitudinal variable expressed in terms of fundamental kinematic variables:

$$y \equiv \frac{1}{2} ln\left(\frac{E + p_z}{E - p_z}\right) \tag{A.5}$$

and it is by definition invariant under Lorentz transformations. In the case that the momentum of a particle is known but not its energy−typically because its mass is unknown−then the pseudo-rapidity $\eta = -ln\left[tan\left(\frac{\theta}{2}\right)\right]$ can be used, where $tan\theta = \frac{\sqrt{x^2+y^2}}{z}$ is the polar angle. It obviously comes that for $p \gg m$ and $p_T \gg m$, $\eta \approx$ y, if one recalls the trigonometric relation $tan\left(\frac{\theta}{2}\right) = \pm\sqrt{\frac{1-cos\theta}{1+cos\theta}}$.

A.3 Multiplicity and centrality

The multiplicity is defined as the number of particles coming from the collision. Often the multiplicity will refer only to the number of charged particles, and should really be called charged particle multiplicity. The multiplicity is often measured differentially as a function of pseudorapidity, $dN/d\eta$ for instance. The charged particle multiplicity at mid-rapidity as a function of energy for pp and A+A collisions is shown in figure A.5. Models that successfully describe RHIC data vary by a factor of two in predicting $dN_{ch}/d\eta|\eta=0$ at the LHC energy. For A+A systems, it is scaled to the number of participant pairs in order to be able to compare between different collision systems and centralities.

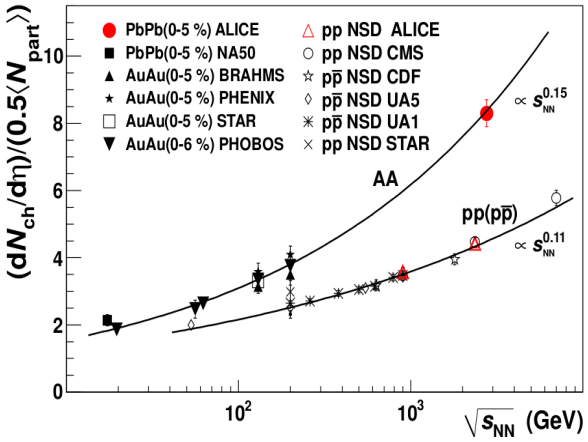

Figure A.5: Charged particle multiplicity at mid-rapidity scaled to the number of participant pairs at different energies and for different collision systems. The LHC data fits the trend from lower energies well[9].

The charged particle pseudorapidity density as a function of η has been measured with the Forward Multiplicity Detector (FMD) and Silicon Pixel Detector (SPD) in ALICE and is presented in figure A.6 and A.7. In the former, $\frac{1}{N_{ev}}\mathrm{d}N_{ch}/\mathrm{d}\eta$ is shown for different centrality classes. For all centrality classes the multiplicity is largest at $|\eta| = 2$. The total charged particle multiplicity integrated from $-y_{beam}$ to y_{beam} is seen in the latter for different centrality bins, here shown by the number of participants (peripheral to more central events). For the most central collision $(0 - 5\%)$ an average of 17 000 charged particles are produced.

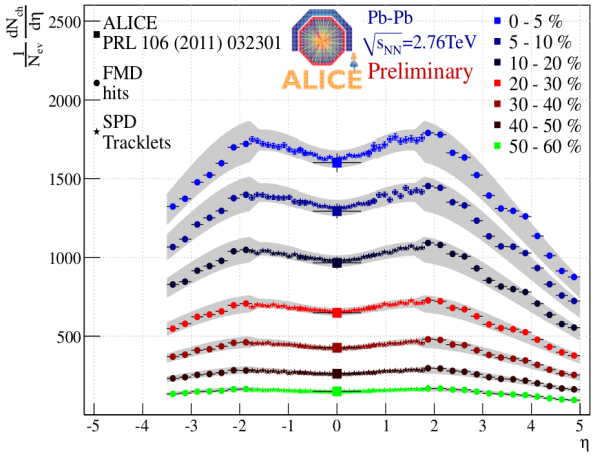

Figure A.6: $\frac{1}{N_{ev}}\mathrm{d}N_{ch}/\mathrm{d}\eta$ for different centrality classes, as measured with the ALICE Forward Multiplicity Detector and Silicon Pixel Detector[11]. The peculiar concave shape has no physical correspondence and accounts for the $\frac{dN_{ch}}{dy} \rightarrow \frac{dN_{ch}}{d\eta}$ transformation.

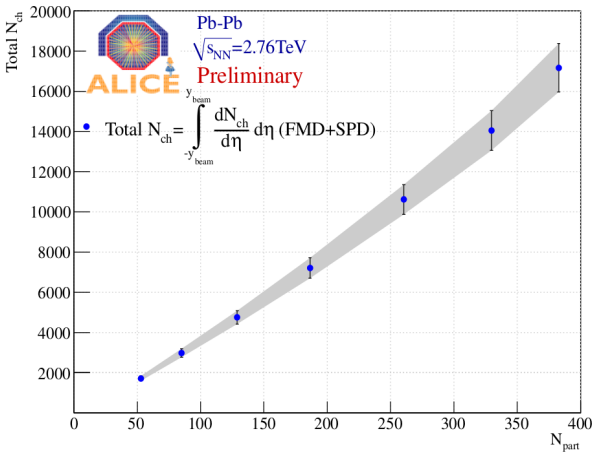

Figure A.7: Integrated charged particle multiplicity N_{ch} for different numbers of participants for Pb+Pb collisions at 2.76 TeV measured with the ALICE Forward Multiplicity Detector and Silicon Pixel Detector. In the most central collisions about 17 000 particles are produced[10].

It is impossible to measure the impact parameter directly. If a larger number of particles participate in the collision, the total multiplicity is increased, thus one can construct a measurement on how central a collision is. The centrality is defined as a number from 0% to 100%, such that a 0% central event has $b \approx 0$, whereas an event with centrality 100% is the most peripheral possible. The slicing in centrality is such that if you choose events with centrality $0 - 10\%$ you will get the top 10% most central events. But determining the centrality from a probability distribution in multiplicity makes the connection to impact parameter non-trivial. In principle it should follow the relation:

$$c = \frac{\int_0^b \frac{d\sigma_{inel}(b)}{db} db}{\sigma_{inel}} \tag{A.6}$$

where σ_{inel} is the total inelastic nuclear cross section and $\frac{d\sigma_{inel}}{db}$ is the differential cross section at impact parameter b. For two identical nuclei the differential cross section becomes $d\sigma_{inel}(b) = 2\pi b db$. Using this and that the maximum impact parameter $b_{max} = 2R$, the total cross section becomes $\sigma_{inel} = 4\pi R^2$, and finally from (A.6) the centrality may be written as

$$c = \frac{b^2}{4R^2} \tag{A.7}$$

For PbPb collisions the latter means that 10% centrality is equal to $b \approx 4.5$ fm. Unfortunately this does not correspond completely to the centrality measured (figure A.8).

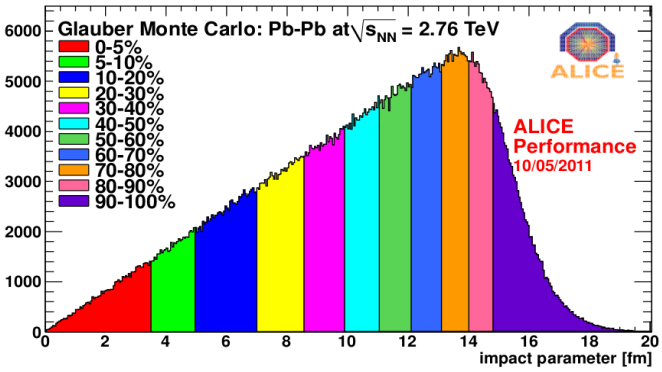

Figure A.8: Centrality determination in ALICE. A Glauber Monte Carlo has been used to visualise impact parameter in centrality slices[8]. Note that the 5% most central events correspond to almost 20% of the total impact parameter range ≈ 14fm, since the 0-5% bin goes up to about 3.5 fm. This is important to keep in mind when looking at plots from the LHC; even though an event has a low centrality, it may not be completely central in terms of impact parameter.

A.4 Vertex topology and V^0 selection criteria

Event and track selection criteria constitute the two major categories of selection criteria *(cuts)*, which in the first case are correlated to the special detector geometry and efficiency, while track selection criteria account for the collision topology and kinematics. Both categories stem from the high standard data acquisition "restrictions" that High Energy field pose. The performance report for the ALICE detector[34] −and the more concentrated article [35] −provide an integrated image of the overall function for the anxious reader.

A schematic of the V^0 vertex topology is presented in figure A.9. The primary vertex[7] distance to the geometrical center of the apparatus is used for the primary event selection. Pertaining to the strange particle (anti-particle) case the selection in order that the former to be identified is applied on the characteristics of their daughter tracks and using their weak decay topology. Weak decays that under consideration are i) $K^0_s \to \pi^+ + \pi^-(B.R. - 69.2\%)$ ii) $\Lambda \to p + \pi^-(B.R. - 63.9)$ and iii) $\bar{\Lambda} \to \bar{p} + \pi^+(B.R - 63.9)$.

The V^0 finding procedure starts with the selection of secondary tracks, i.e. tracks having a sufficiently large impact parameter with respect to the primary vertex (DCA_p). All possible combinations between two secondary tracks of opposite charge are examined and accepted as V^0 candidates only if the distance between them (DCA_s) is smaller than 0.5 cm. The V^0 vertex position (secondary vertex) is a point on the DCA_s line. Its distance from each daughter track is taken to be proportional to the precision of the track parameter estimations. Once their position is determined, only the V^0 candidates located inside a volume, corresponding to an inner radius of 0.2 cm and an outer limit of 100 cm from the primary vertex, are kept. In particular, for Λ and $\bar{\Lambda}$ reconstruction, the V^0 finding procedure checks whether the particle momentum $\vec{p}$ (calculated based on momentum conservation as the summation of the track momenta extrapolated to the DCA_s position) associated with the V^0 candidate points back to the primary vertex. This is achieved by applying a cut on the cosine> 0.99 of the angle pointing angle $\vartheta_{\vec{p}}$ between $\vec{p}$ and a vector connecting the primary vertex and the V^0 position (V^0 line of flight).

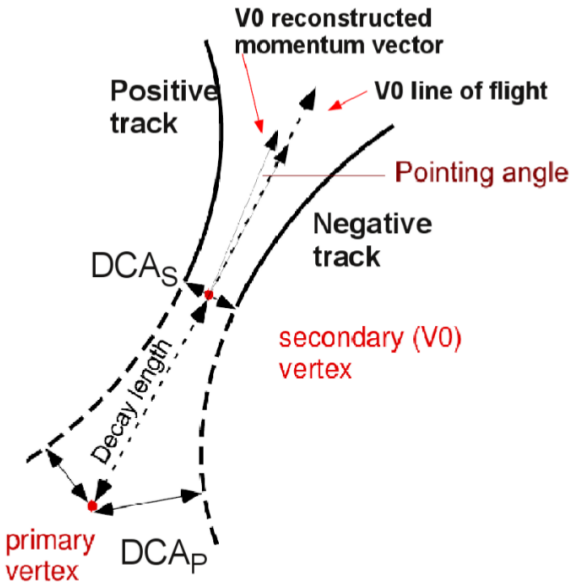

Figure A.9: V^0 vertex topology; solid line represent the reconstructed tracks of the alleged daughter particles in which the initial V^0 decays. The V shape araising from the opposite directions that the charged daughter particles follow due to magnet existence in cases like the one depicted accounts for the V^0 notation.

A.5 The Data

The data used in this analysis comprised of two sets. In the determination of v_2 for charged particles 452 518 events(DATA set 1) were used, while for the identified particle cases 1 355 755 events (DATA set 2) coming from LHC10h. Both are raw data, whose number notation (10) corresponds to the year of data taking (2010) and the letter holds for the specific time period inside the respective year. The ATLAS plots were constructed via entries provided by the online database Durham HepData Project.

[7] The reconstructed collision point.

A.6 Figures

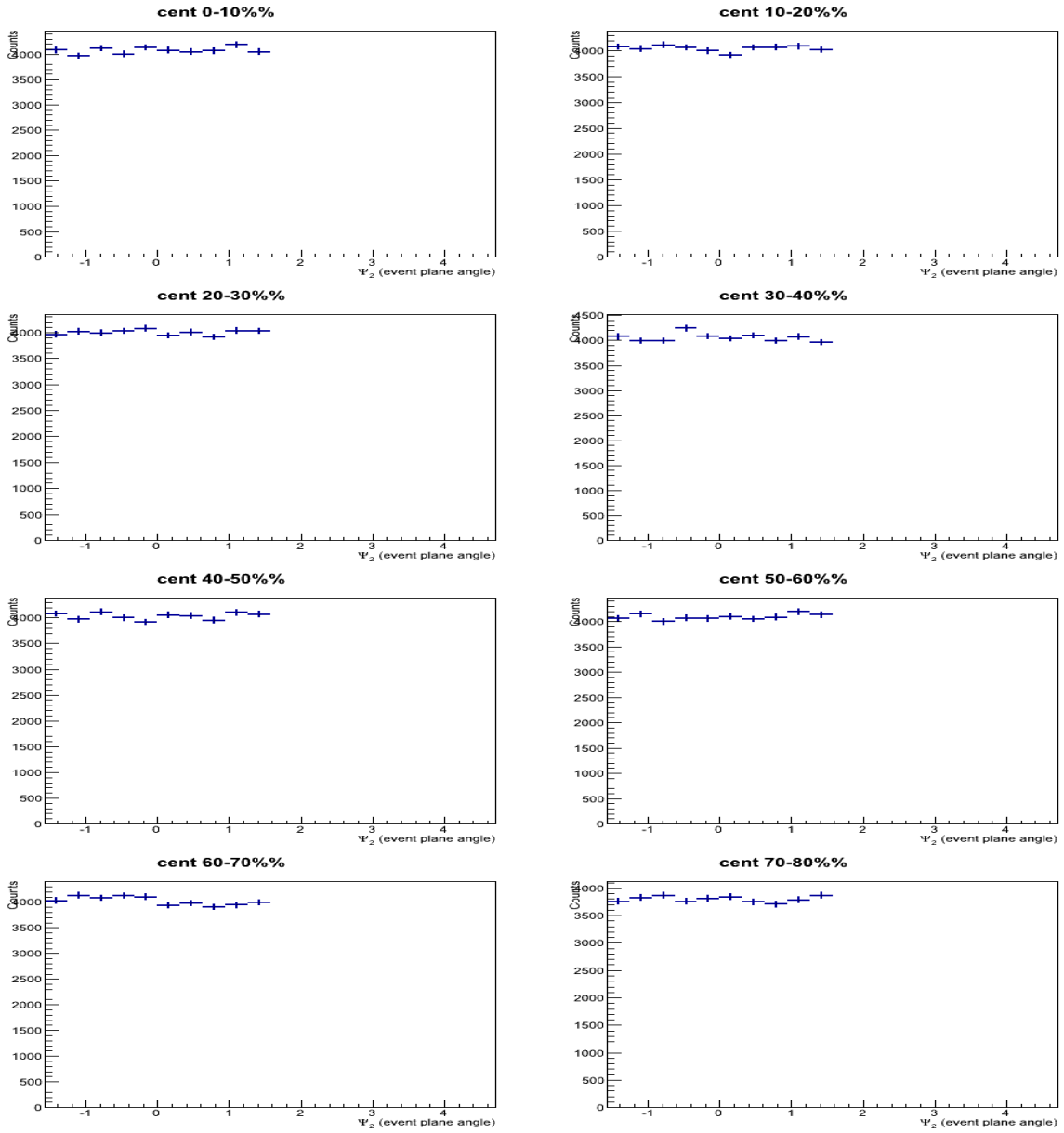

Figure A.10: Azimuthal distribution of the event plane based on DATA set 1.

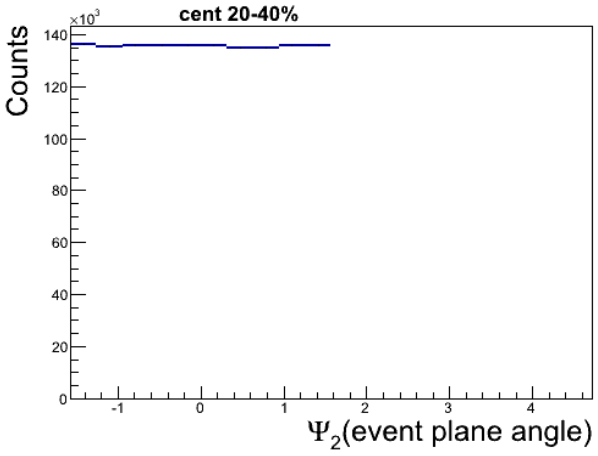

Figure A.11: Azimuthal distribution of the event plane based on DATA set 2 for comparison.

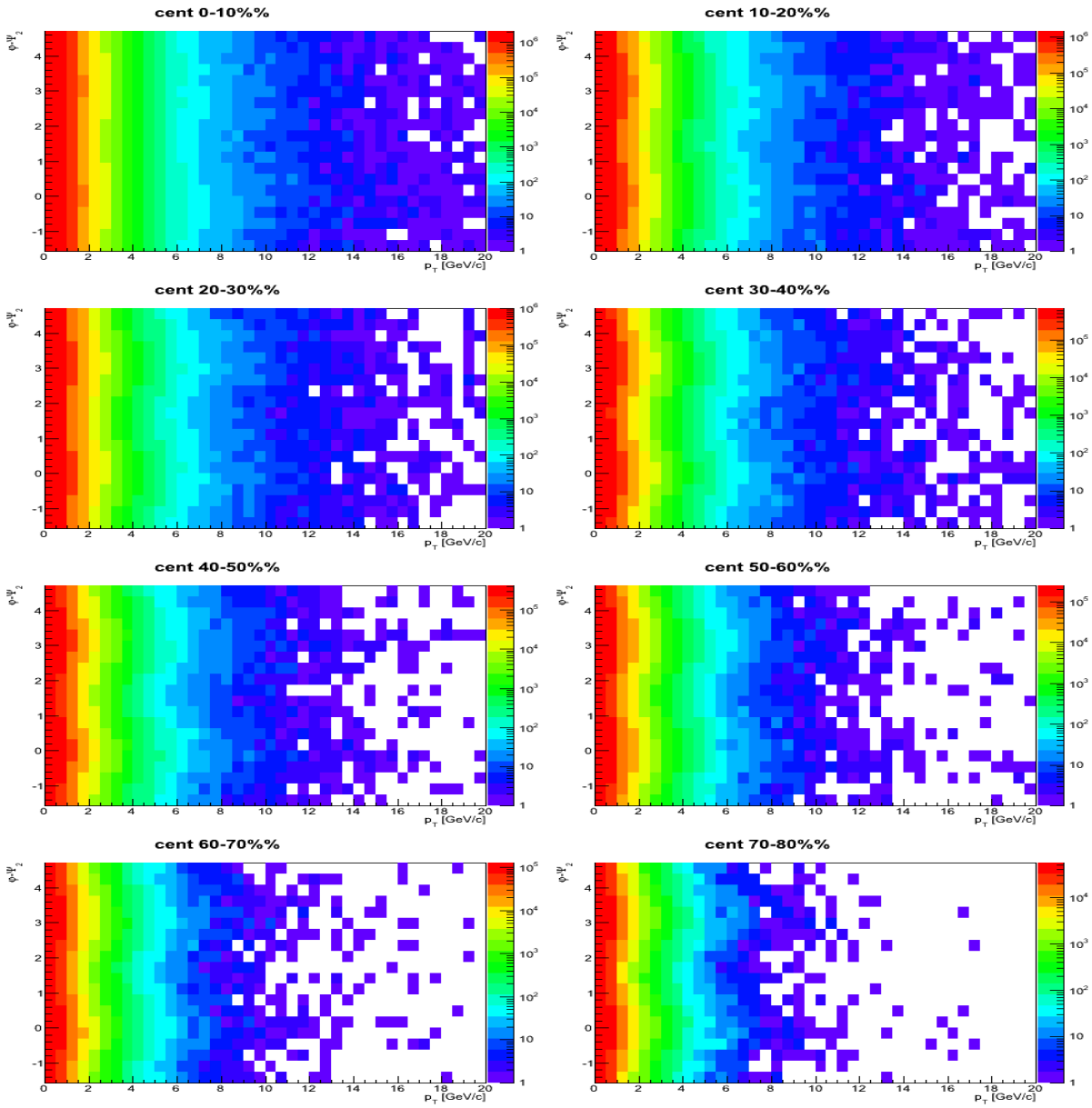

Figure A.12: Azimuthal distributions with respect to the reconstructed reaction plane Ψ_2 momentum for eight centrality bins. The sinusoidal patterns could be distinguished indicating maximum values(the ones approaching the upper limits in the color band) at 0 and π rad for each p_T bin.

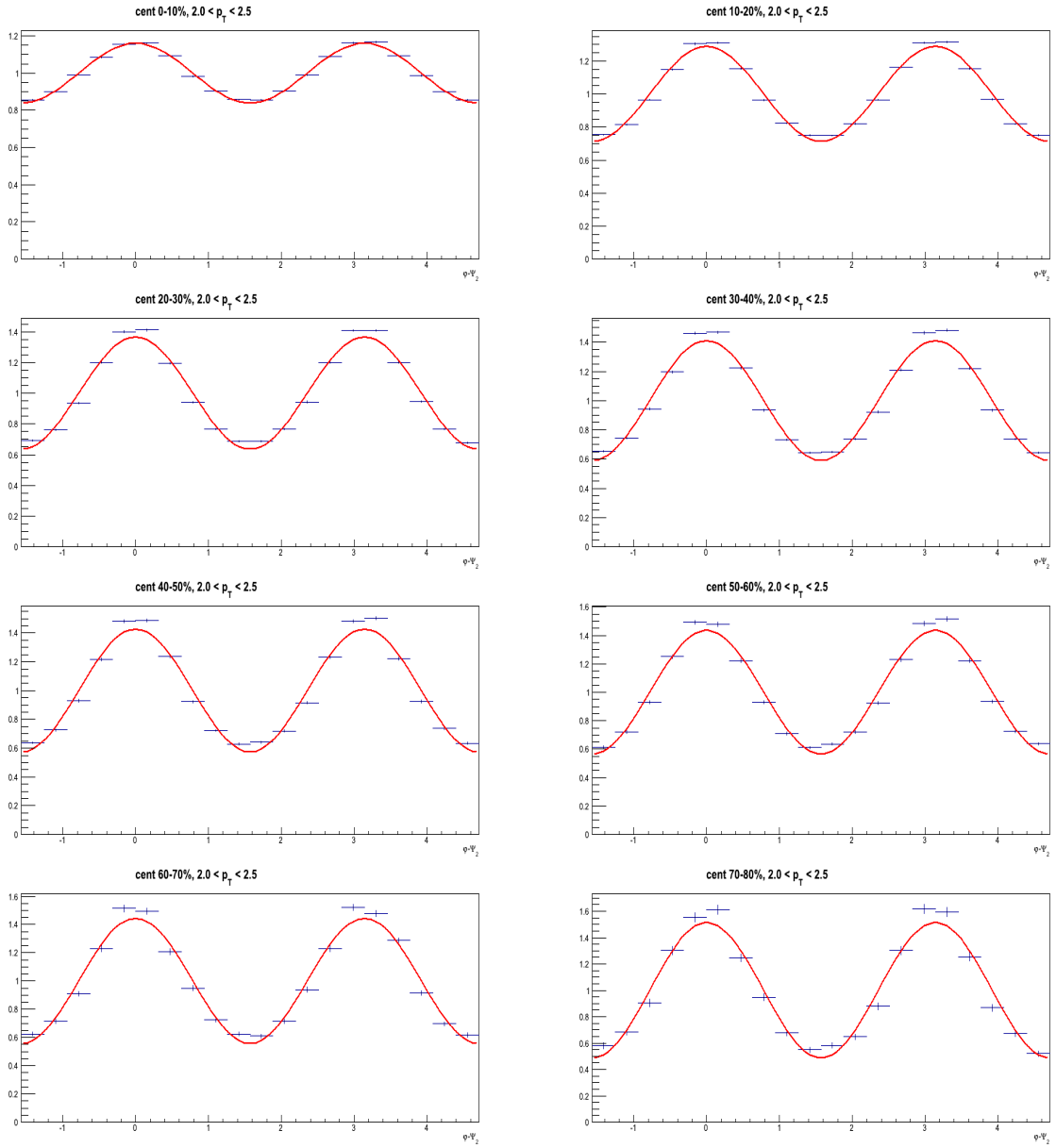

Figure A.13: Distribution of the azimuthal angle relative to the measured event plane angle in eight centrality intervals for $2 \leq p_T \leq 2.5 GeV$.

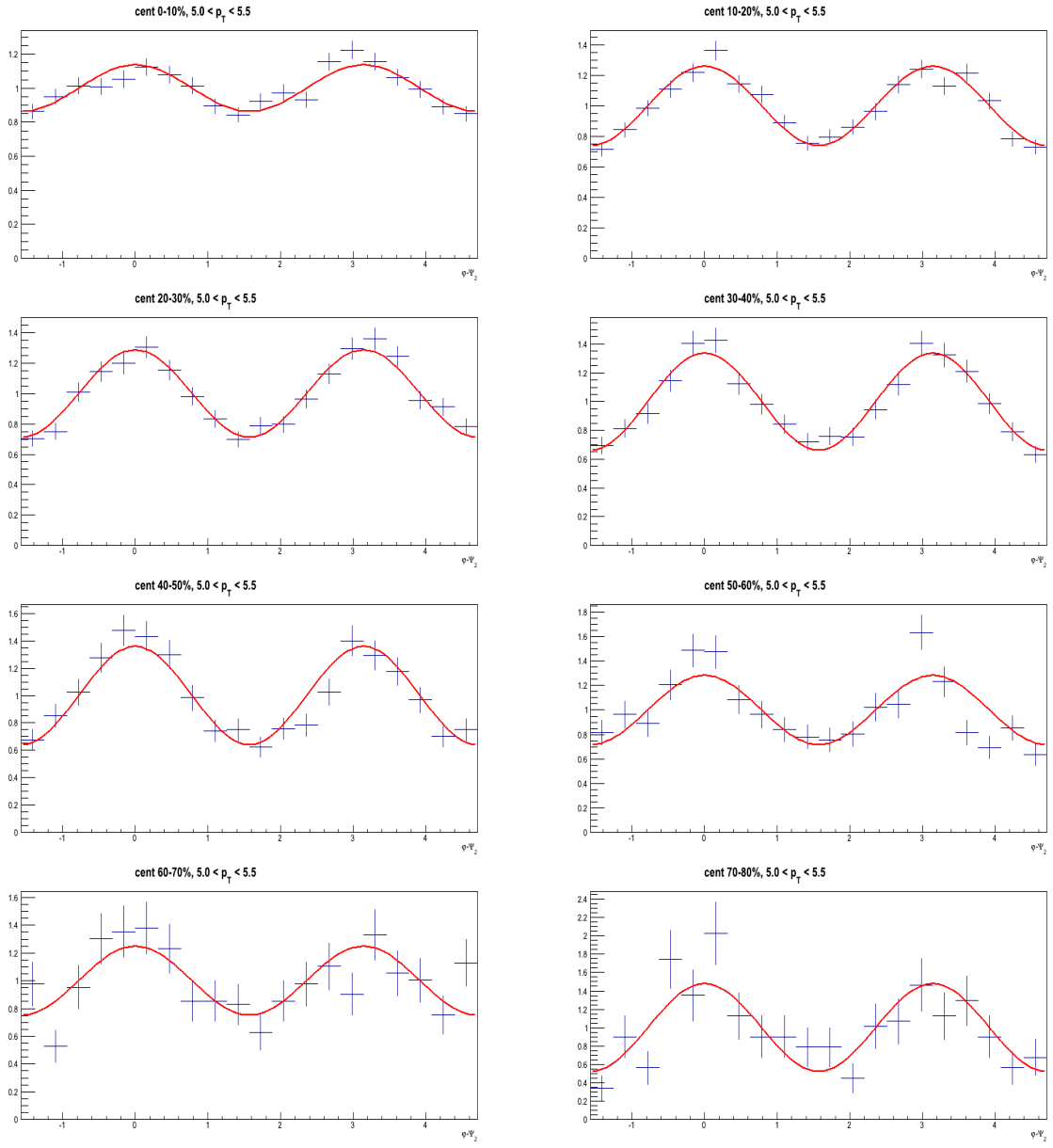

Figure A.14: Distribution of the azimuthal angle relative to the measured event plane angle in eight centrality intervals for $5 \leq p_T \leq 5.5 GeV$.

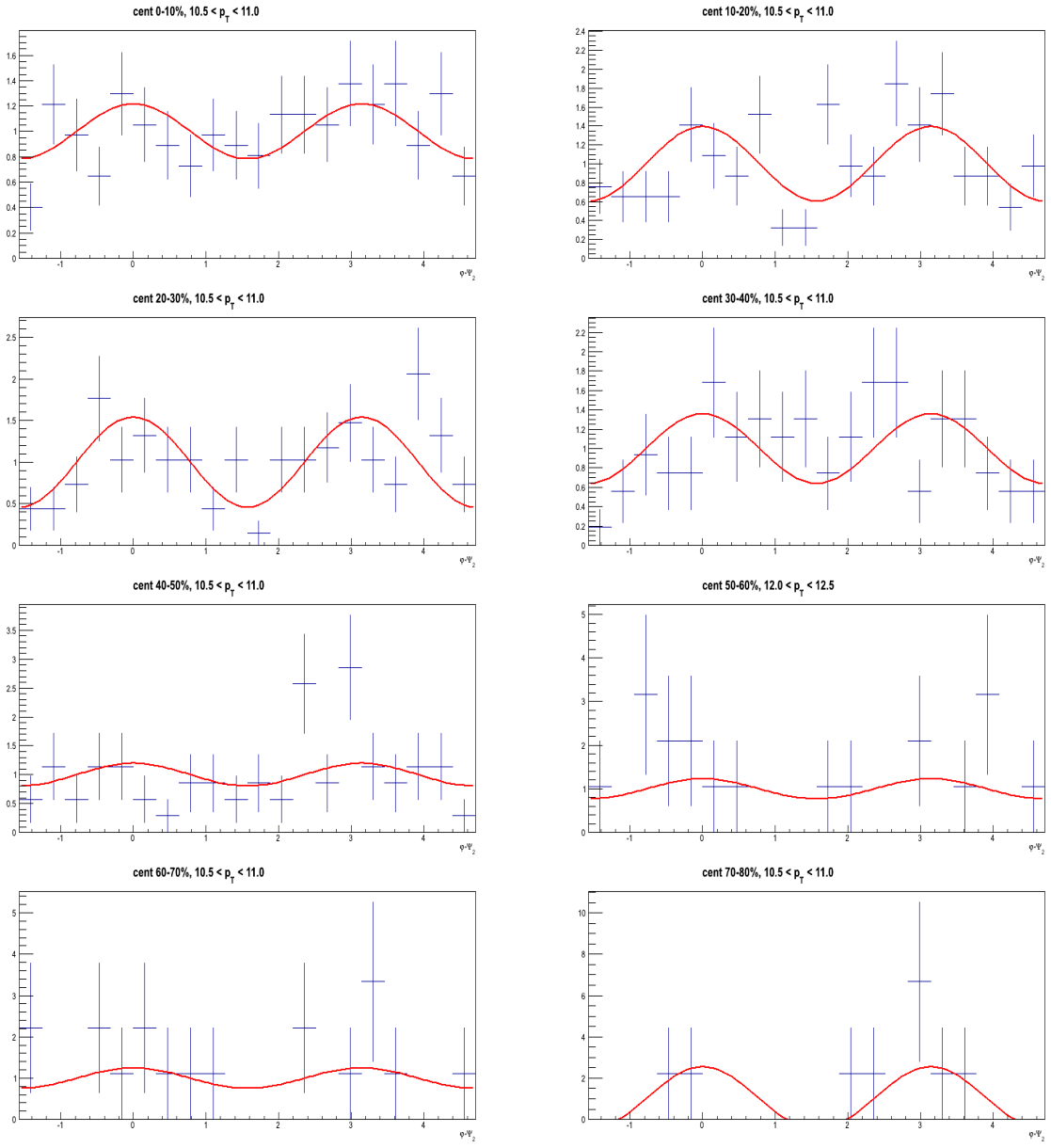

Figure A.15: Distribution of the azimuthal angle relative to the measured event plane angle in eight centrality intervals for $10.5 \leq p_T \leq 11 GeV/c$. In the bottom right panel fitting does not converge due to low statistics.

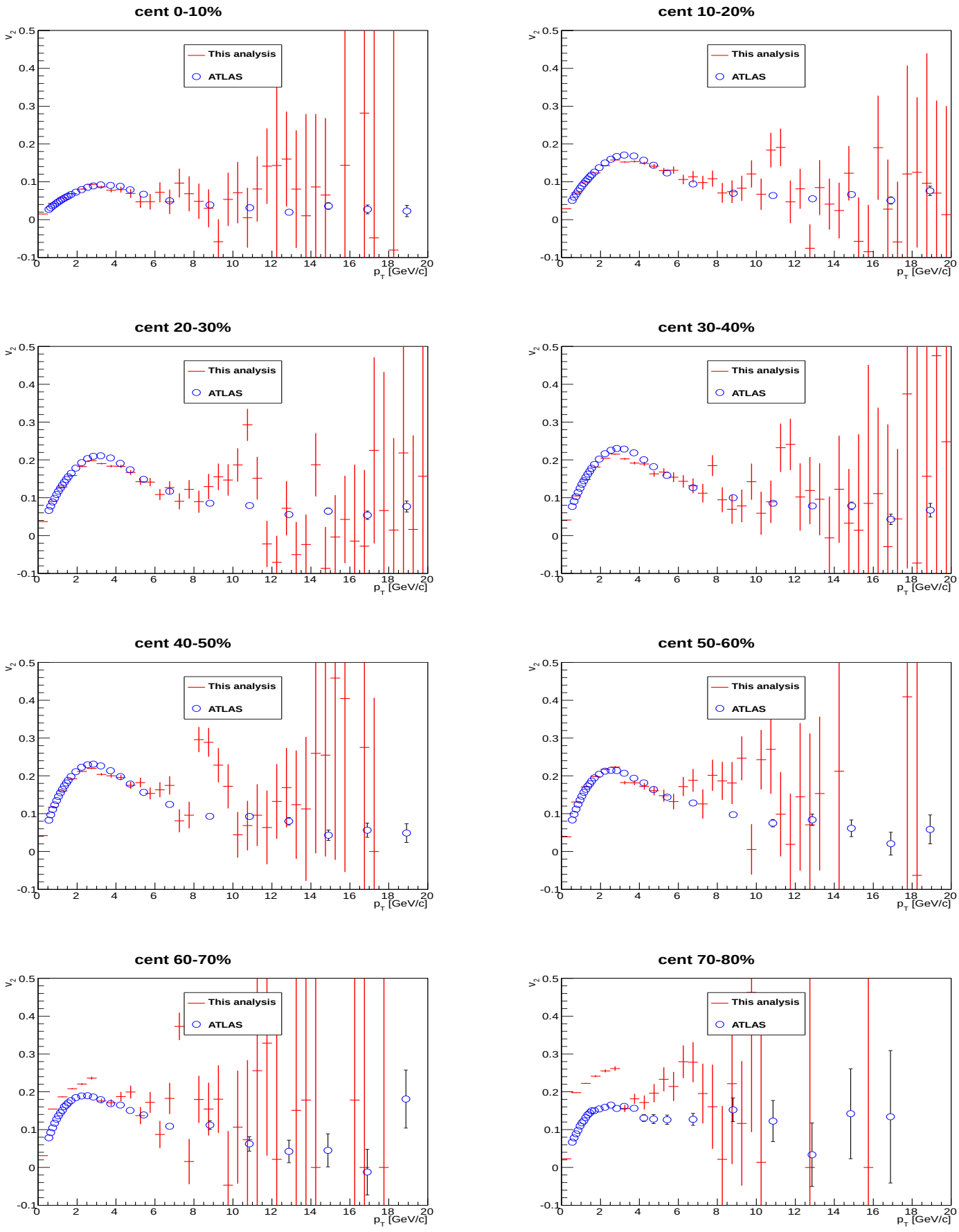

Figure A.16: Elliptic flow $v_2(p_T)$ as a function of p_T for eight 10% centrality intervals, for p_T from 0.5 to 20 GeV/c. Results compared to ATLAS experiment[5]

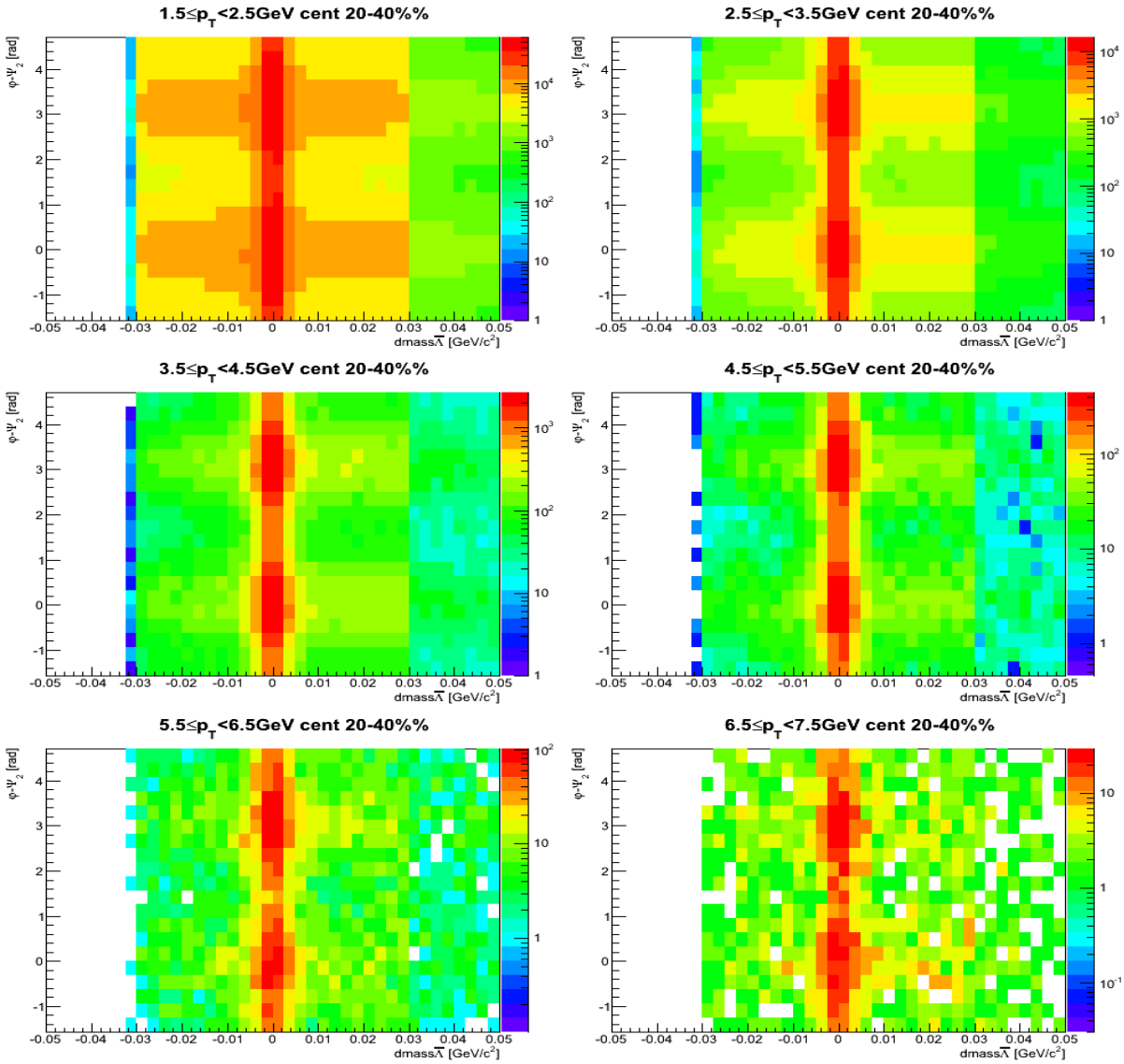

Figure A.17: Azimuthal distributions with respect to the reconstructed reaction plane Ψ_2 invariant mass for $\bar{\Lambda}$ up to $p_T <$ 7.5GeV/c. Elliptic flow is evident– maximum values at 0 and π rad.

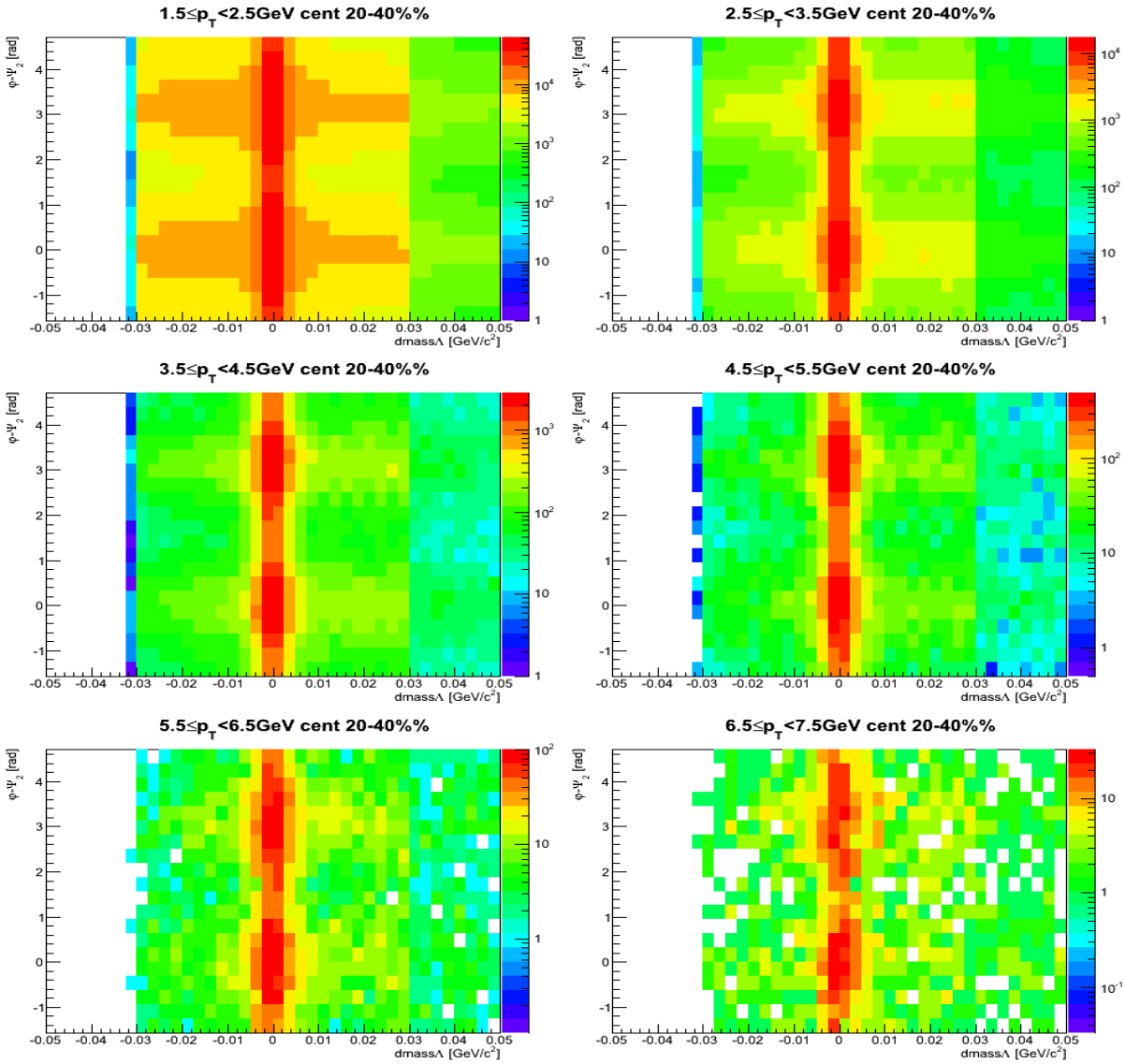

Figure A.18: Azimuthal distributions with respect to the reconstructed reaction plane Ψ_2 invariant mass for Λ up to $p_T <$ 7.5GeV/c. Elliptic flow is evident– maximum values at 0 and π rad.

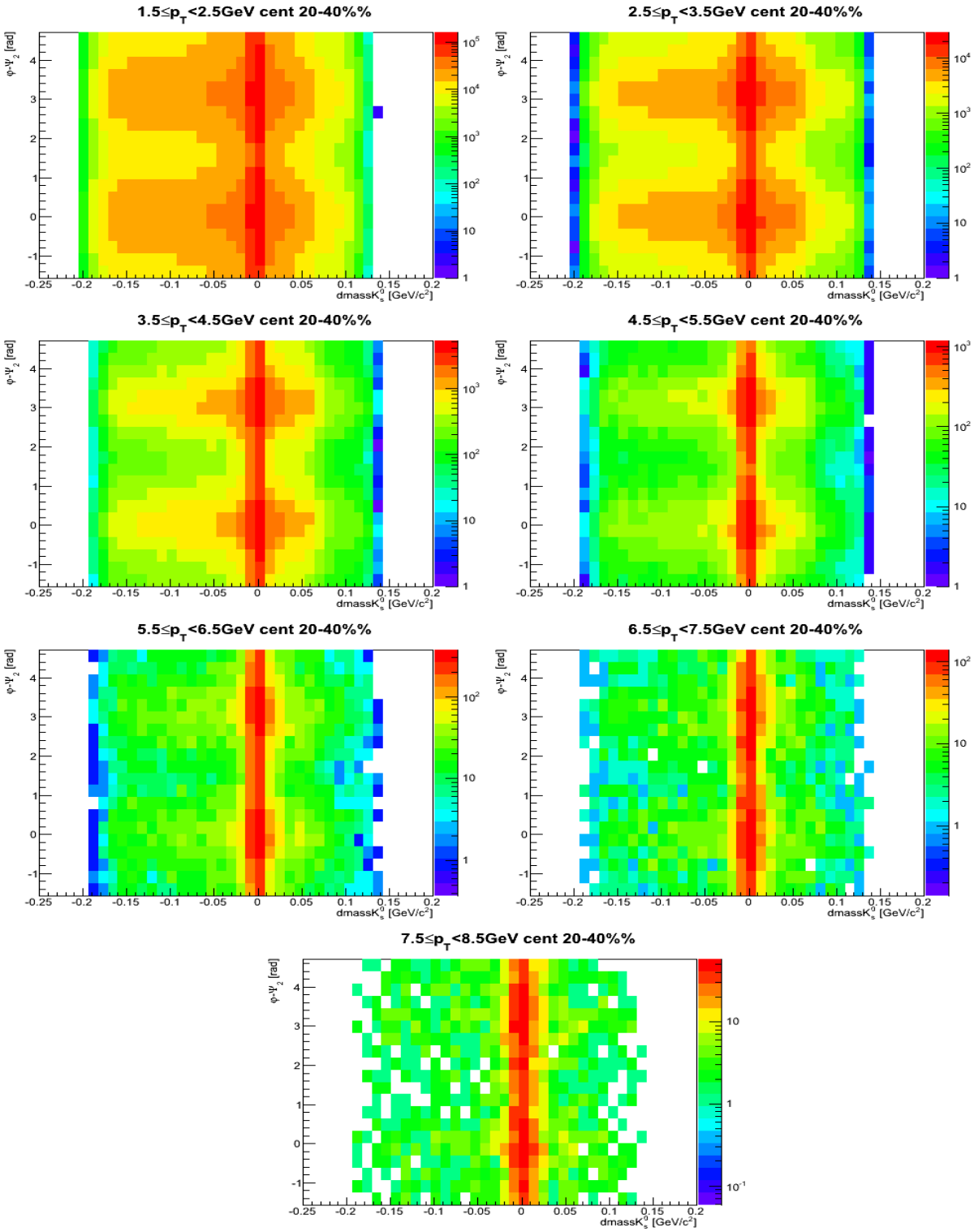

Figure A.19: Azimuthal distributions with respect to the reconstructed reaction plane Ψ_2 invariant mass for K^0_s up to $p_T < 8.5$GeV/c. Elliptic flow is evident– maximum values at 0 and π rad.

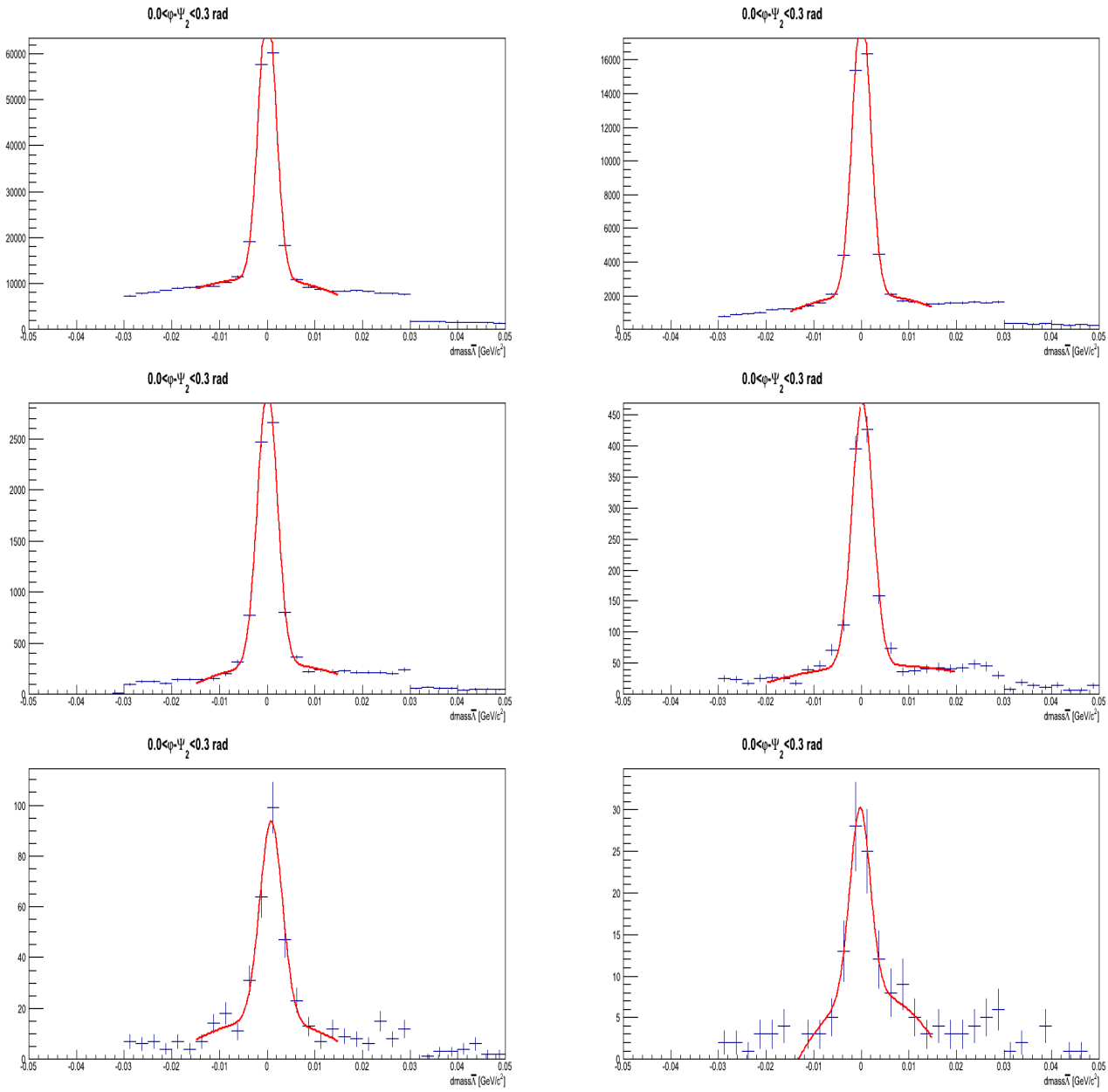

Figure A.20: Invariant mass fitting based on (5.3) for $\bar{\Lambda}$ near 0 rad in the $1.5 \leq p_T < 7.5$ GeV/c(from ridge to bottom panel). The rest fittings are skipped.

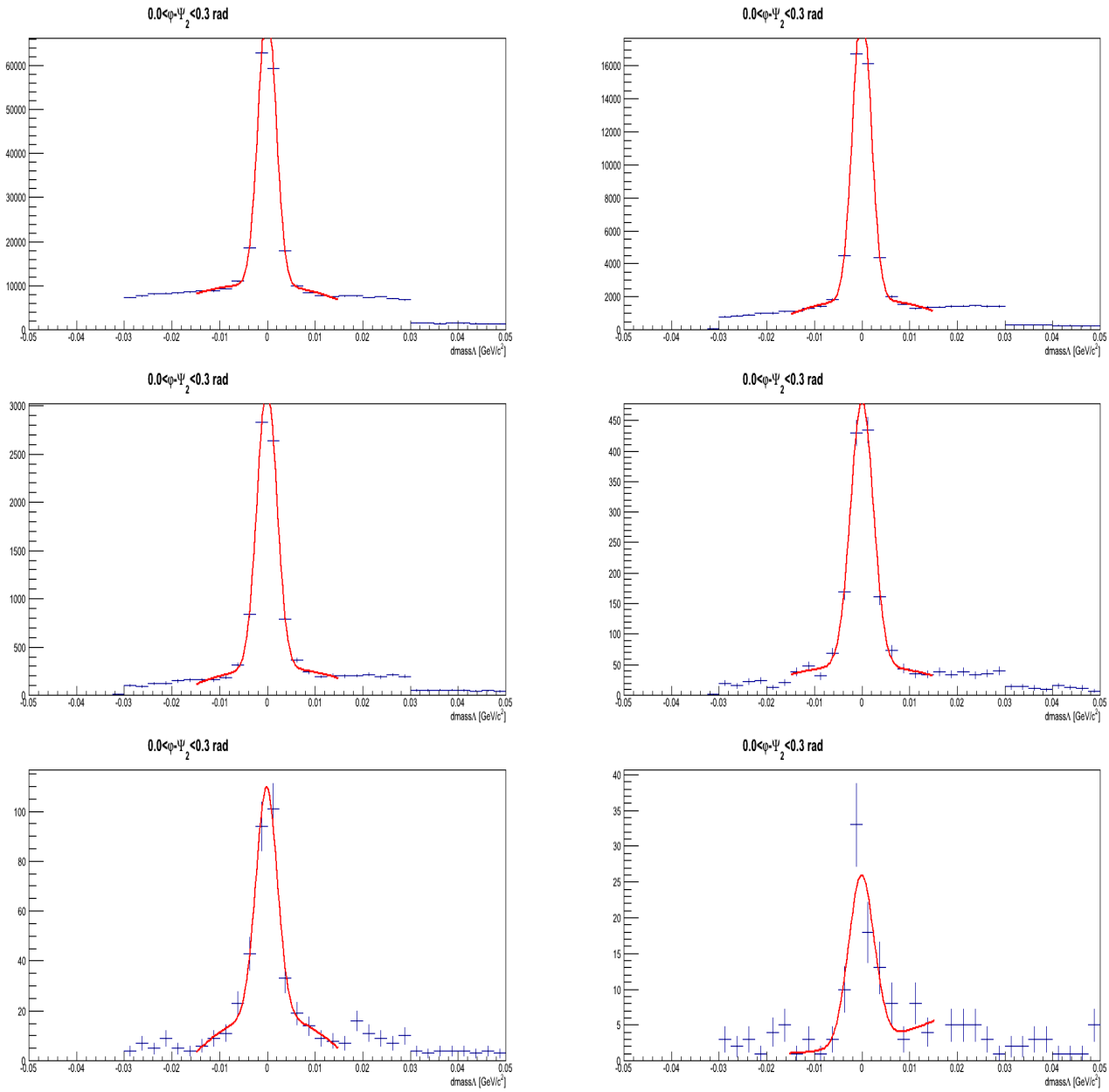

Figure A.21: Invariant mass fitting based on (5.3) for Λ near 0 rad in the $1.5 \leq p_T < 7.5$ GeV/c(from ridge to bottom panel). Deviations from experimental points with increasing centrality where fitting parametrization fails to reproduce them are expected, such as in the bottom panel. The rest fittings are skipped.

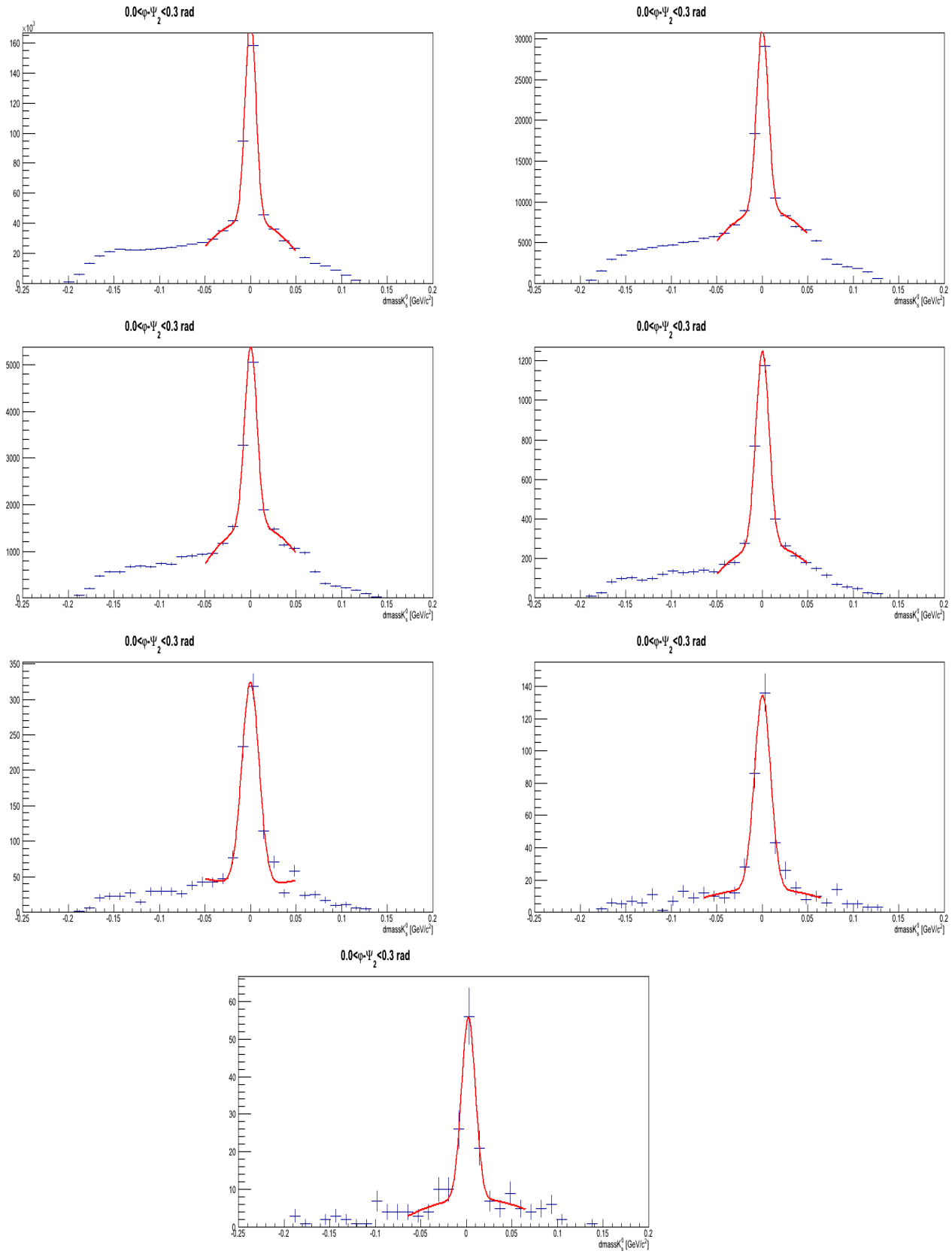

Figure A.22: Invariant mass fitting based on (5.3) for K_s^0 near 0 rad in the $1.5 \leq p_T < 8.5$ GeV/c(from ridge to bottom panel). The rest fittings are skipped.

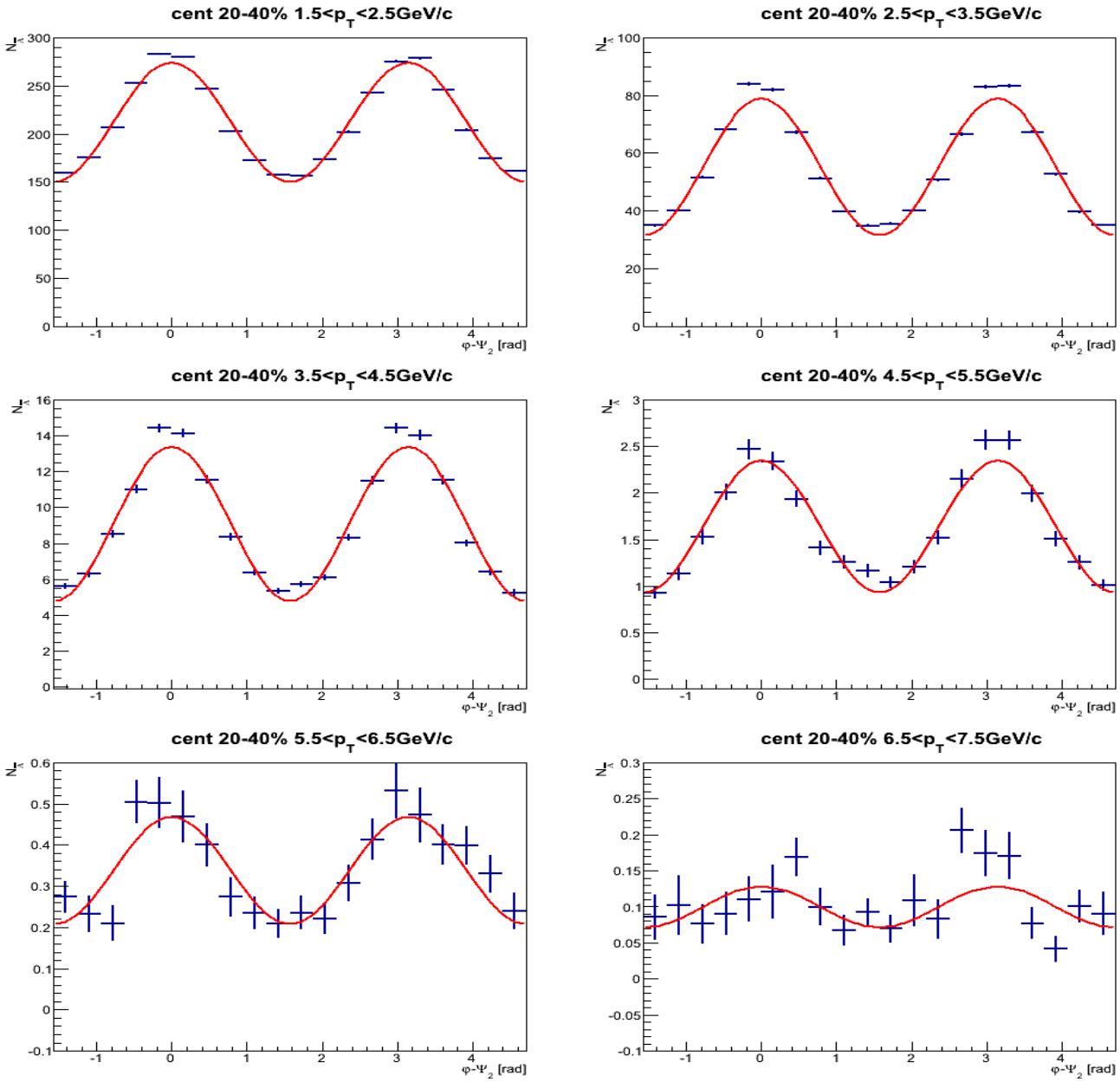

Figure A.23: Number of produced $\bar{\Lambda}$ anti-particles(*yield*) relative to the event plane angle Ψ_2. Maximum values are observed in-plane(0 and π rad respectively), while miminum values stand for out-of- plane direction($-\frac{\pi}{2}$, $\frac{\pi}{2}$ and $\frac{3\pi}{2}$ rad).

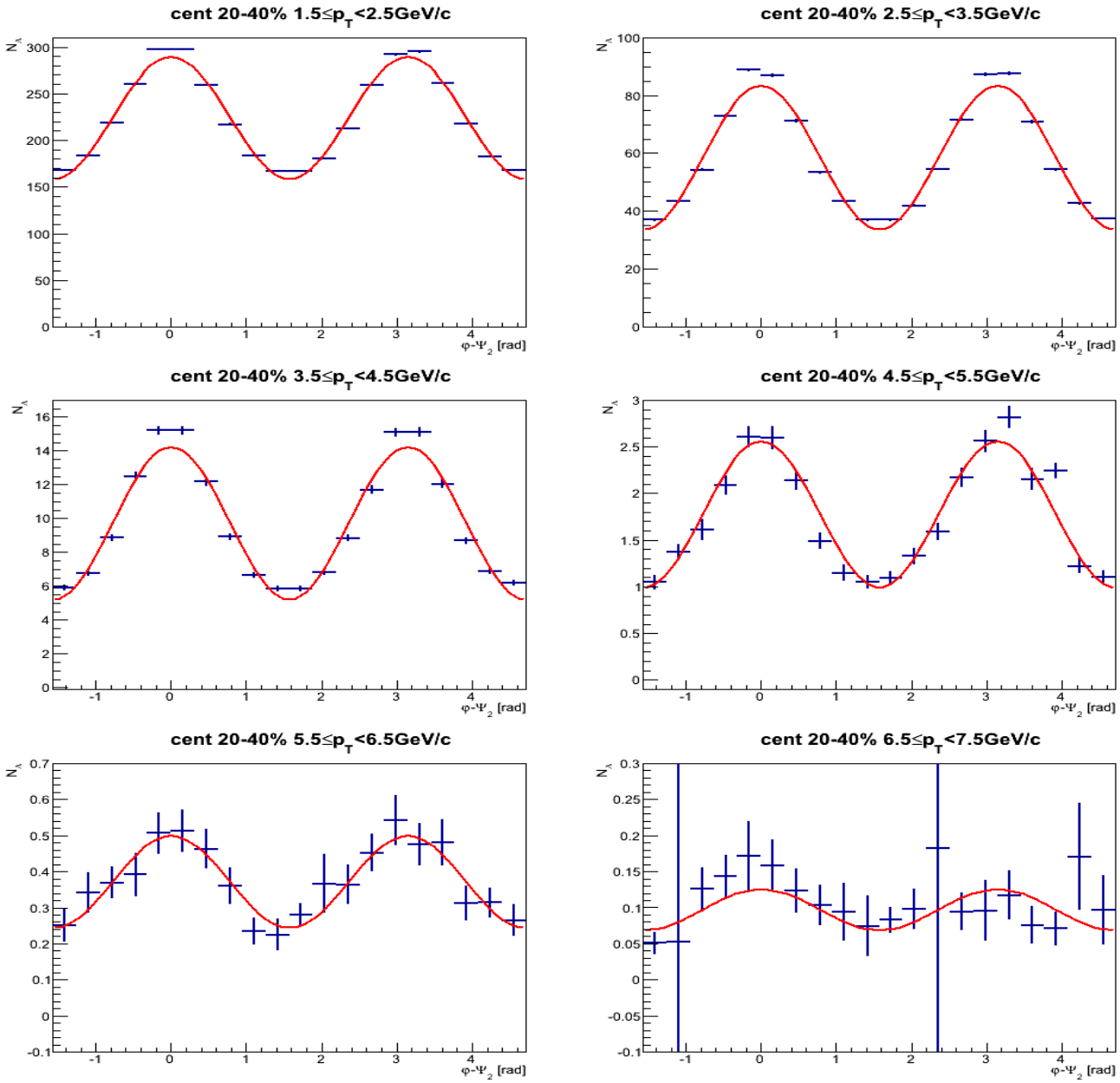

Figure A.24: Number of produced Λ baryons(*yield*) relative to the event plane angle Ψ_2. Maximum values are observed in-plane(0 and π rad respectively), while miminum values stand for out-of- plane direction($-\frac{\pi}{2}$, $\frac{\pi}{2}$ and $\frac{3\pi}{2}$ rad).

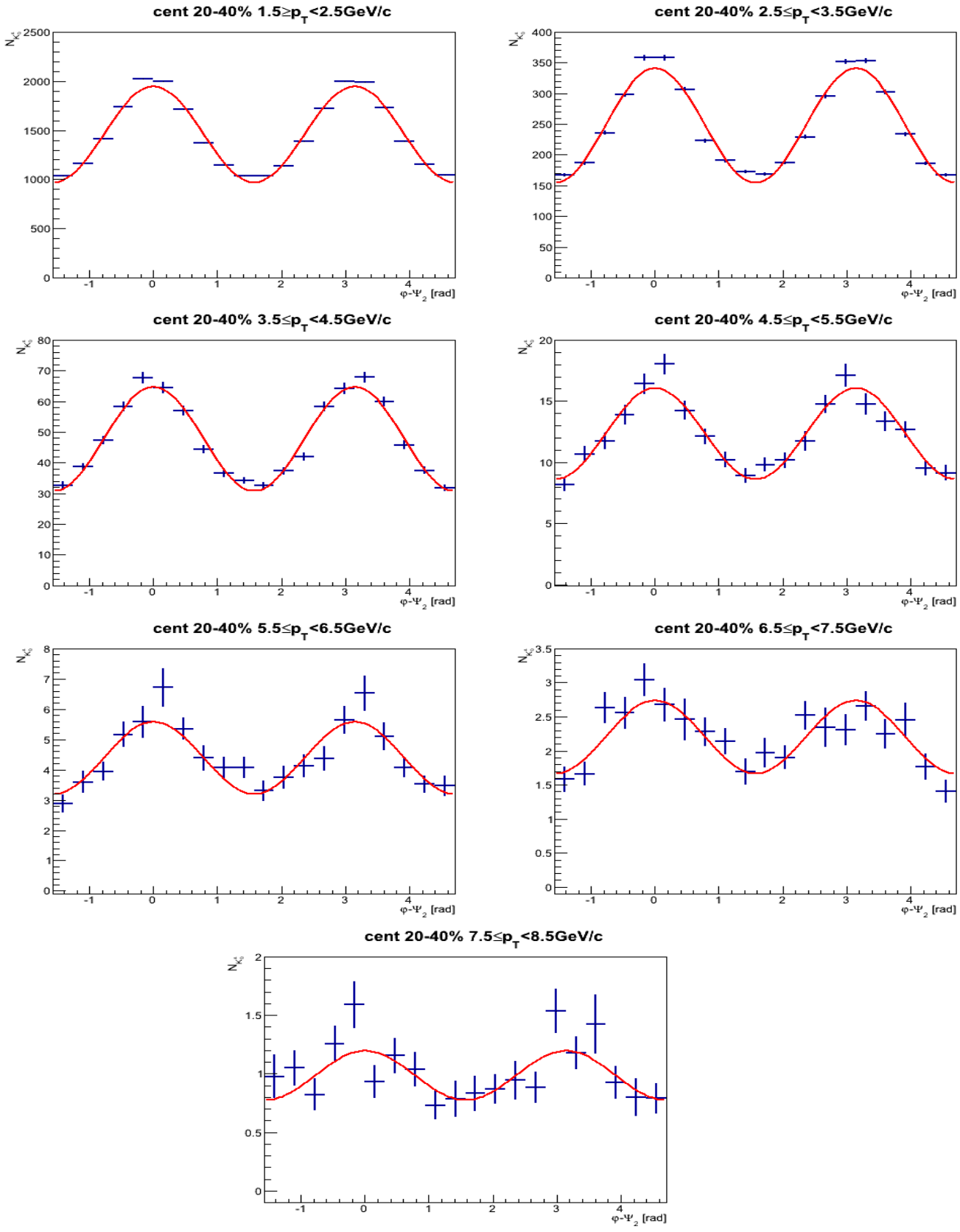

Figure A.25: Number of produced K_s^0 mesons(*yield*) relative to the event plane angle Ψ_2. Maximum values are observed in-plane(0 and π rad respectively), while miminum values stand for out-of- plane direction($-\frac{\pi}{2}$, $\frac{\pi}{2}$ and $\frac{3\pi}{2}$ rad).

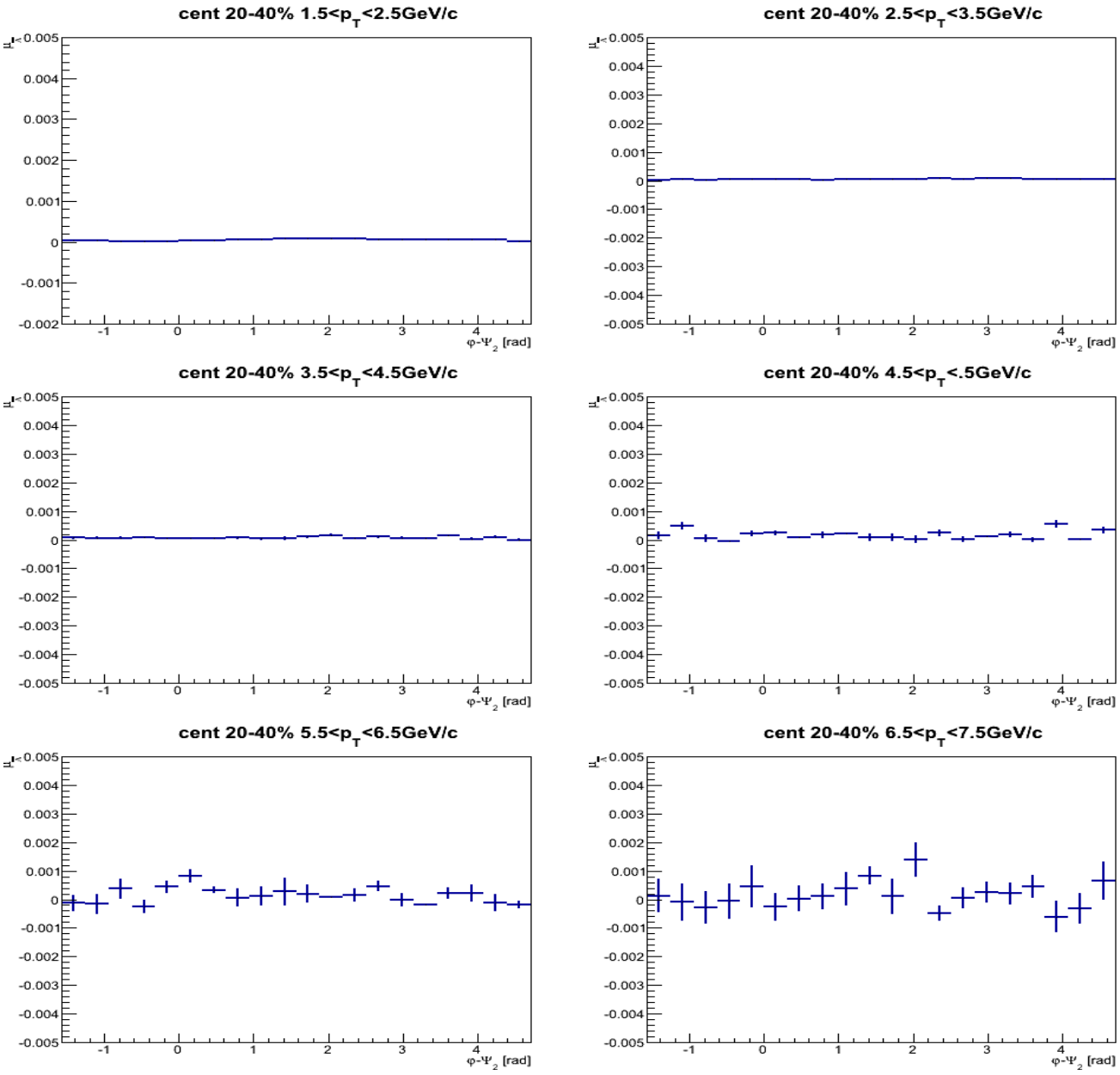

Figure A.26: Mean value of the invariant mass fitting for $\bar{\Lambda}$−parameter [1] in (5.3); it should be around zero.

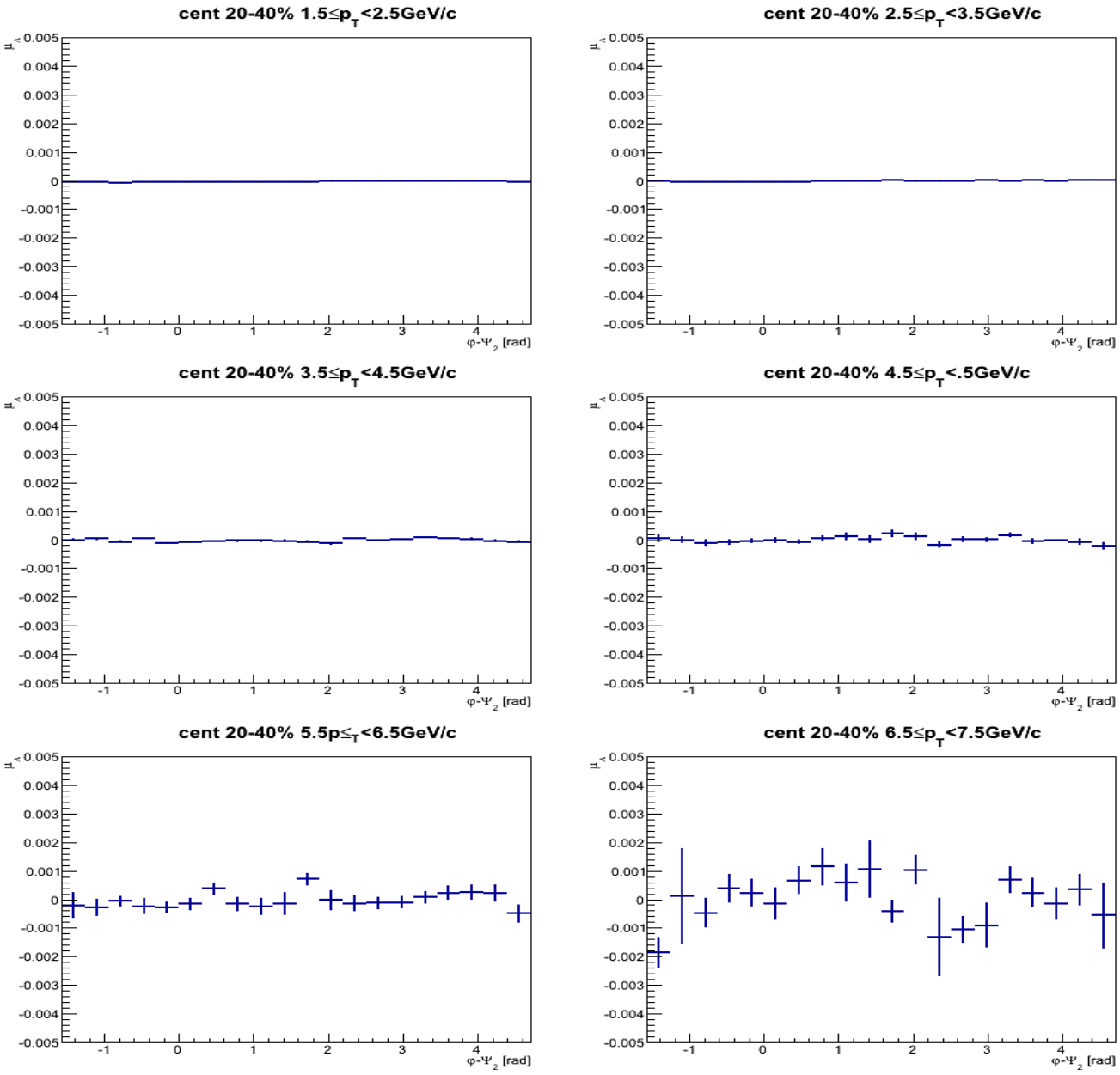

Figure A.27: Mean value of the invariant mass fitting for Λ−parameter [1] in (5.3); it should be around zero.

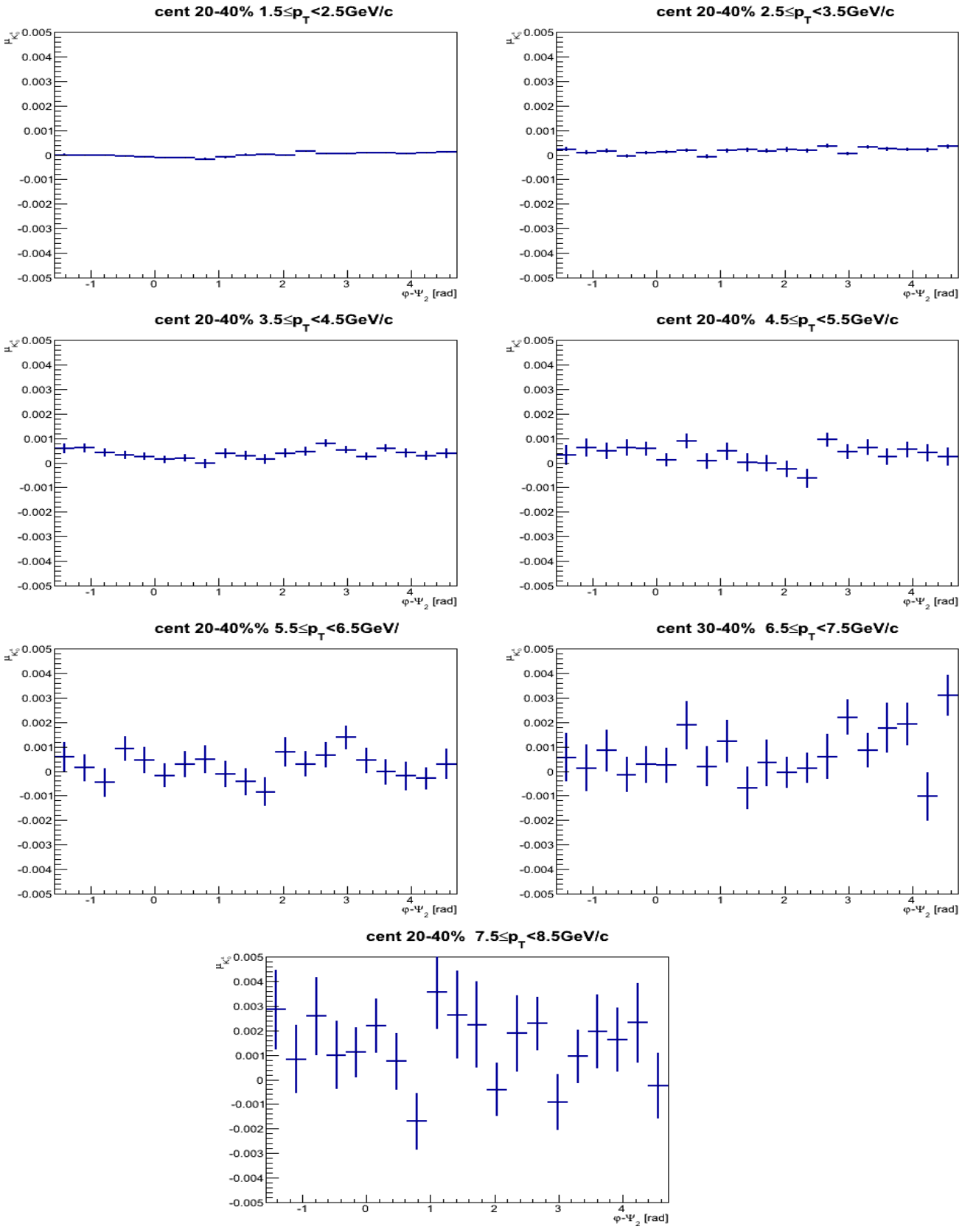

Figure A.28: Mean value of the invariant mass fitting for K_s^0-parameter [1] in (5.3); it should be around zero.

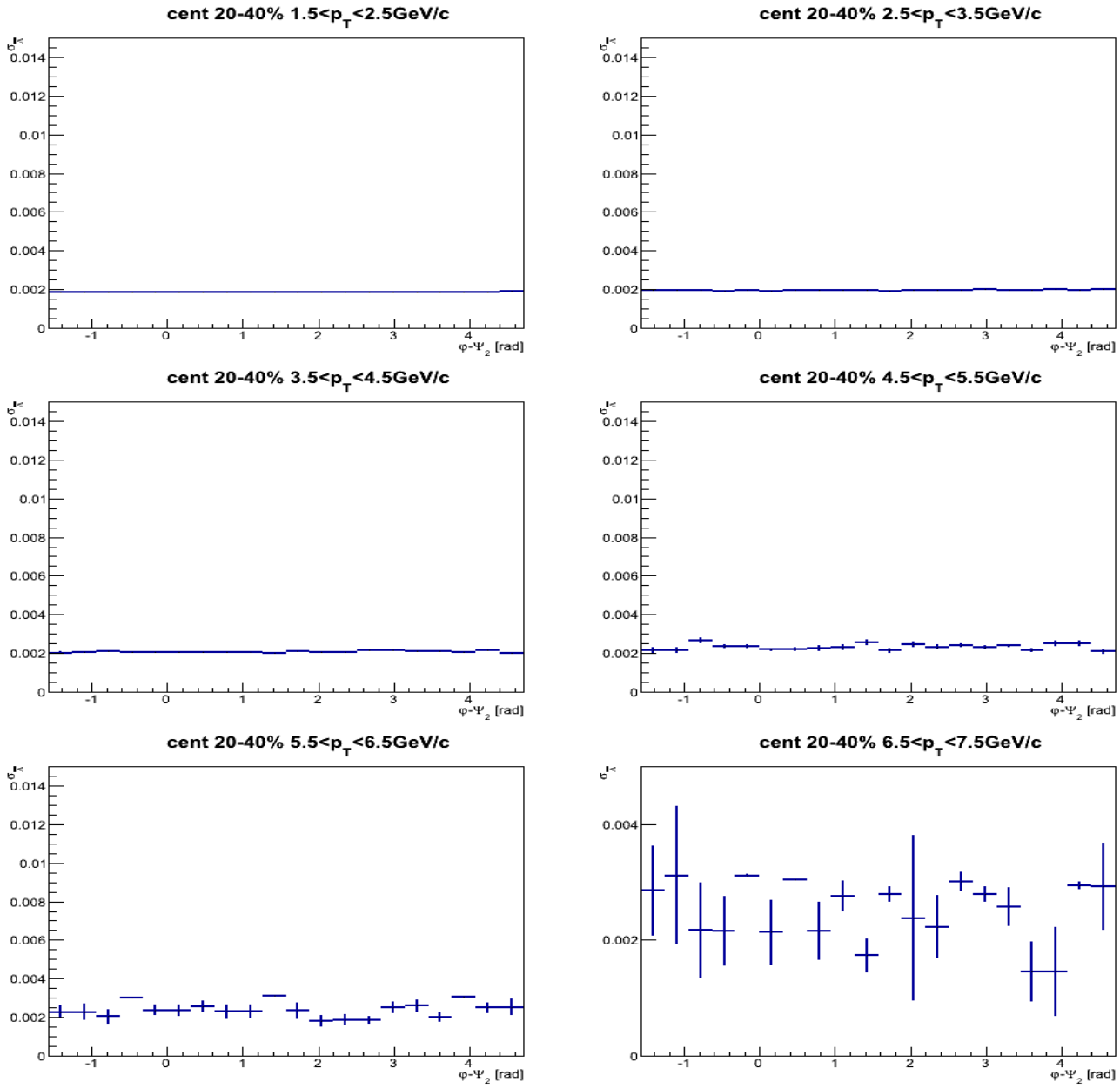

Figure A.29: Sigma value of the invariant mass fitting for $\bar{\Lambda}$−parameter [2] in (5.3); it should be flat.

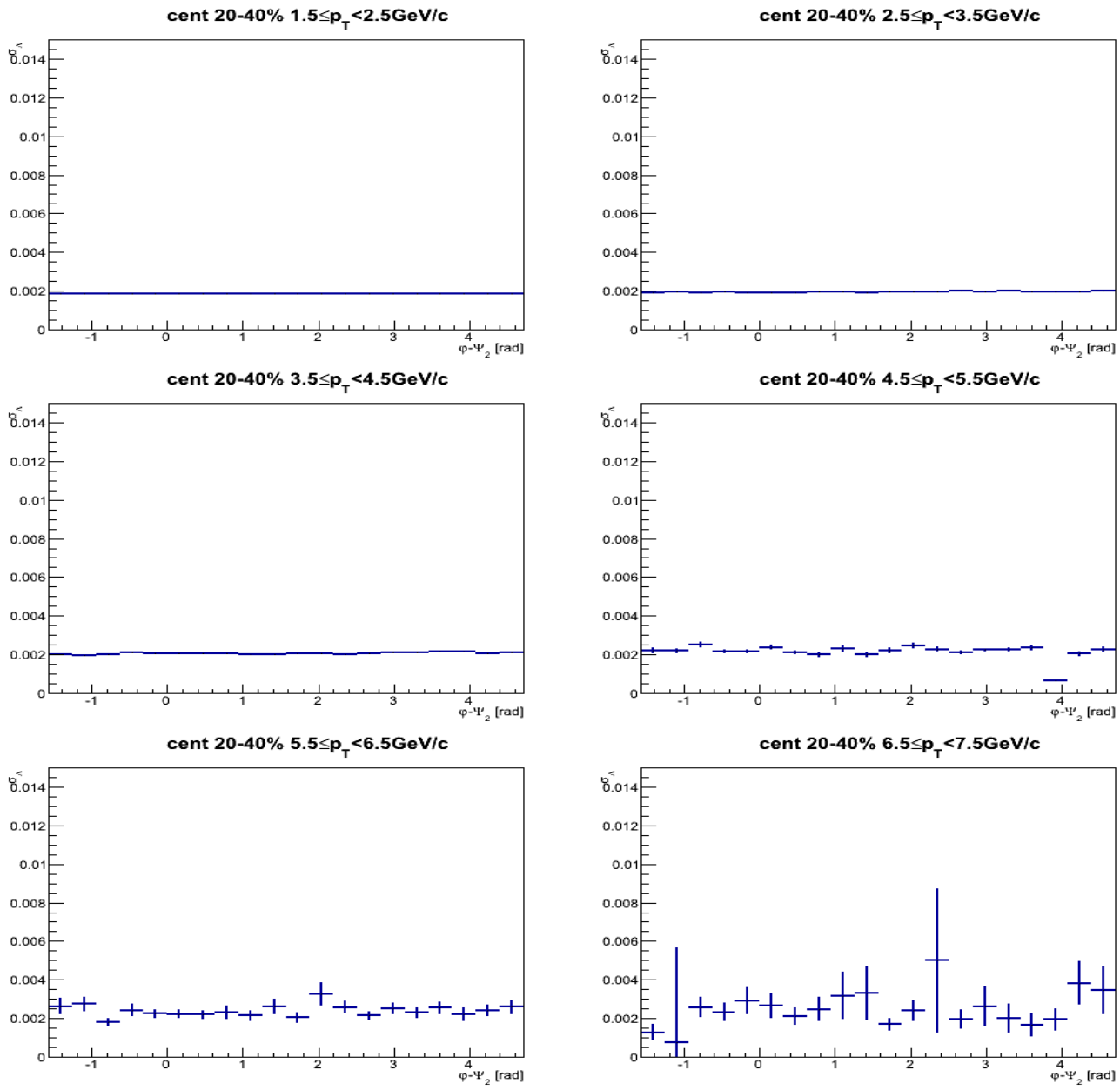

Figure A.30: Sigma value of the invariant mass fitting for Λ−parameter [2] in (5.3); it should be flat.

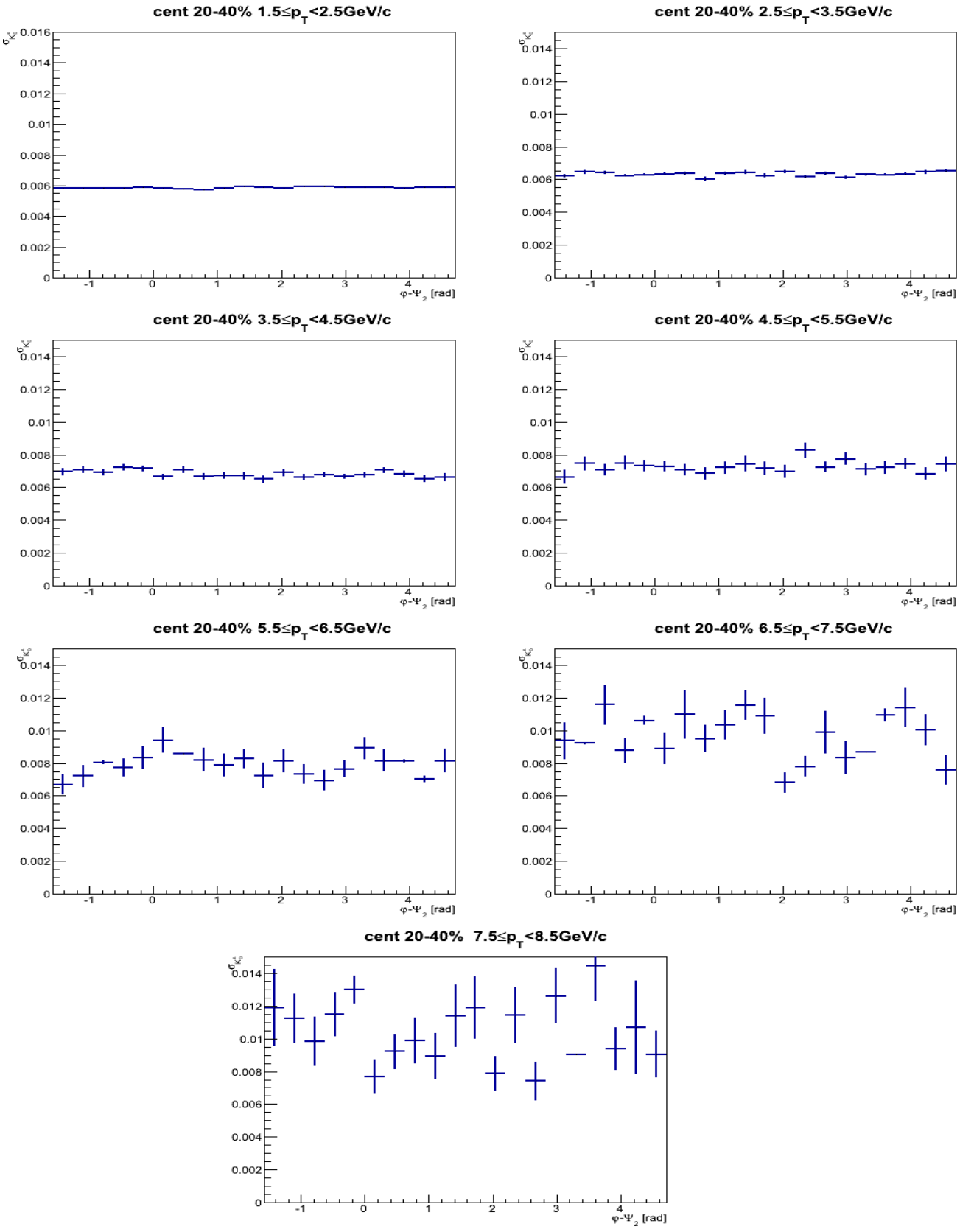

Figure A.31: Sigma value of the invariant mass fitting for K_s^0−parameter [2] in (5.3); it should be flat.

References

[1] S. Voloshin, Y.Zhang, *Flow Study in Relativistic Nuclear Collisions by Fourier Expansion of Azimuthal Particle Distributions*, Z.Phys.,**vol.C70**,(1996),pp.665-672

[2] *Hydrodynamical assessment of 200A GeV collisions,* Ekkard Schnedermann and Ulrich Heinz, Phys. Rev. D,**vol. 48**,(1993),pp. 2462–2476

[3] B. Alver, M. Baker, C. Loizides and P. Steinberg, *The PHOBOS Glauber Monte Carlo,* arXiv:0805.4411(2008)

[4] Jean-Yves Ollitrault, *Anisotropy as a signature of transverse collective flow*, Phys. Rev. D, **vol. 46**(1992) pp. 229–245

[5] ATLAS collaboration, *Measurement of the pseudorapidity and transverse momentum dependence of the elliptic flow of charged particles in lead-lead collisions at* $\sqrt{s_{NN}}$ *= 2.76 TeV with the ATLAS detector*, arXiv:1108.6018(2012)

[6] A. Andronic et al., *Excitation function of elliptic flow in Au+Au collisions and the nuclear matter equation of state*,Phys.Lett. B.,**vol.612**,(2005),pp. 173–180

[7] H. H. Dalsgaard, *The Forward Multiplicity Detector for ALICE*, M.S. thesis, University of Copenhagen, (2007)

[8] Alberica Toia for the ALICE Collaboration, *Bulk Properties of Pb-Pb collisions at* $\sqrt{s_{NN}}$ *= 2.76 TeV measured by ALICE*, Presented at Quark Matter 2011, Annecy, France(2011).

[9] K. Aamodt et al., *Charged-particle multiplicity density at mid-rapidity in central Pb-Pb collisions at* $\sqrt{s_{NN}}$ *= 2.76 TeV*, Phys.Rev.Lett., **vol. 105**,(2010),pp. 252301

[10] Alberica Toia for the ALICE Collaboration, *Bulk Properties of Pb-Pb collisions at = 2.76 TeV measured by ALICE*, arXiv:1107.1973 [nucl-ex],(2011)

[11] H. H. Dalsgaard, Ph.D. thesis, University of Copenhagen, (2011)

[12] ROOT| A Data Analysis Framework

[13] M. Demoulins *et al.*, *Measurement of a Baryon azimuthal emission pattern in Ne+(NaF, Nb, Pb) collisions at 800 MeV per nucleon*, Physics Letters B, **vol. 241**, (1990),pp. 476-480

[14] E.V.Shuryak,*Quantum chromodynamics and the theory of superdense matter,*Phys.Rep., **vol.61**,71(1980)

[15] Paul Richard Sorensen,*Kaon and Lambda Production at Intermediate* p_T*: Insights into the Hadronization of the Bulk Partonic Matter Created in Au+Au Collisions at RHIC,* Ph.D. Thesis arXiv:nucl-ex/0309003v2(2003)

[16] Paul Sorensen, *Highlights from Heavy Ion Collisions at RHIC and the Acoustics of the Little Bangs*, arXiv:1201.0784v1 [nucl-ex]

[17] M. L. Miller, K. Reygers, S. J. Sanders and P. Steinberg, *Glauber Modeling in High Energy Nuclear Collisions*, Ann. Rev. Nucl. Part. Sci., **vol. 57**,205,(2007),*arXiv:nucl-ex/0701025v1*

[18] D. Teaney, J. Lauret, E.V. Shuyak, *A Hydrodynamic Description of Heavy Ion Collisions at the SPS and RHIC*, (2001),*arXiv:nucl-th/0110037v2*

[19] N. Borghini, P. M. Dinh, and J.-Y. Ollitrault, *Flow analysis from multiparticle azimuthal correlations,* Phys. Rev. C **vol. 64**, 054901 (2001).

[20] J. Adams et al. STAR Collaboration, *Azimuthal anisotropy in Au+Au collisions at* $\sqrt{s_{NN}}$*=200 GeV*, Phys. Rev. C, **vol. 72**, 014904 (2005)

[21] Mike Miller, Raimond Snellings, *Eccentricity fluctuations and its possible effect on elliptic flow measurements*, (2003),arXiv:nucl-ex/0312008v2

[22] Sergei A. Voloshin, Arthur M. Poskanzer, Raimond Snellings,*Collective Phenomena in Non-Central Nuclear Collisions*,(2008),arXiv:0809.2949v2 [nucl-ex]

[23] A. M. Poskanzer and S. A. Voloshin,*Methods for analyzing anisotropic flow in relativistic nuclear collisions* ,Phys. Rev. C, **vol.58** (1998), pp.1671–1678

[24] Martin, Brian, and Graham Shaw, THE BREIT-WIGNER FORMULA, in *Particle Physics*, (Chippenham, Wiltshire,Great Britain:Antony Rowe Ltd, 2008), pp. 351-355

[25] B. B. Back et al. PHOBOS Collaboration,*Centrality and pseudorapidity dependence of elliptic flow for charged hadrons in Au+Au collisions at* $\sqrt{s_{NN}}$*=200 GeV*,Phys. Rev. C, **vol.72**, 051901(R) (2005)

[26] Miklos Gyulassy, Ivan Vitev, Xin-Nian Wang, Pasi Huovinen,*Transverse expansion and high pT azimuthal asymmetry at RHIC*,Physics Letters B, **vol. 526**,(2002), pp. 301-308

[27] Rainer Fries, Vincenzo Greco, and Paul Sorensen,*Coalescence Models for Hadron Formation from Quark-Gluon Plasma*, Annual Review of Nuclear and Particle Science, **vol.58** (2008)pp.177-205,annurev.nucl.58.110707.171134

[28] Raimond Snellings (the STAR and ALICE Collaboration),*Anisotropic Flow from RHIC to the LHC*,(2006)arXiv:nucl-ex/0610010v1

[29] P. Huovinen, P.F. Kolb, U. Heinz, P.V. Ruuskanen, S.A. Voloshin,*Radial and elliptic flow at RHIC: further predictions*,Physics Letters B,**vol. 503**,(2001),pp.58-64

[30] C. Adler et al.[STAR Collaboration],*Elliptic flow from two- and four-particle correlations in Au+Au collisions at* $\sqrt{s_{NN}}$*=130GeV*,Phys. Rev. C,**vol.66**, 034904 (2002)

[31] STAR Collaboration,*Mass, quark-number, and* $\sqrt{s_{NN}}$ *dependence of the second and fourth flow harmonics in ultra-relativistic nucleus-nucleus collisions*, Phys.Rev.C.,**vol.75**,054906,(2007)

[32] W.A.Zajc,*The Fluid Nature of Quark-Gluon Plasma*,Nucl.Phys.A,**vol.805**,(2008),pp.283-294

[33] Nu Xu, Masashi Kaneta,*Hadron freeze-out conditions in high energy nuclear collisions*,Nucl.Phys. A.,**vol.698** (2002),pp. 306-313

[34] ALICE Collaboration,*ALICE: Physics Performance Report, Volume I*,J. Phys. G: Nucl. Part. Phys. **30** 1517(2004)

[35] ALICE Collaboration, *Strange particle production in proton-proton collisions at* $\sqrt{s_{NN}}$*= 0.9 TeV with ALICE at the LHC*,Eur.Phys.J.C,**vol.71**:1594,(2011)

[36] P. Danielewicz, G. Odyniec,*Transverse momentum analysis of collective motion in relativistic nuclear collisions*,Physics Letters B,**vol.157**(1985),pp.146-150

[37] K. Aamodt et al. (ALICE Collaboration),*Elliptic Flow of Charged Particles in Pb-Pb Collisions at* $\sqrt{s_{NN}} = 2.76$ *TeV*,Phys. Rev. Lett.,**vol.105**, 252302(2010)

[38] H.H. Gutbrod, K.H. Kampert, B.W. Kolb, A.M. Poskanzer, H.G. Ritter, H.R. Schmidt,*A new component of the collective flow in relativistic heavy-ion collisions*,Physics Letters B,**vol.216**,(1989),pp.267-271

[39] A. Adare et al. PHENIX Collaboration,*Dihadron azimuthal correlations in Au+Au collisions at √sNN=200 GeV* , Phys. Rev. C.,**vol.78**,014901(2008)

[40] The STAR Collaboration,*Azimuthal Charged-Particle Correlations and Possible Local Strong Parity Violation*,Phys.Rev.Lett.,**vol.103**,251601(2009)

[41] Alexander Colliander Hansen, Pseudorapidity Dependence of Elliptic Flow in Pb+Pb Collisions at $\sqrt{s_{NN}}$ = 2.76TeV with ALICE, Master's Thesis, Niels Bohr Institute, University of Copenhagen(2011)

[42] S.A. Voloshin, A.M. Poskanzer,*The physics of the centrality dependence of elliptic flow*,Physics Letters B, **vol.474**, (2000),pp. 27-32

[43] Berndt Muller, Jurgen Schukraft, Bolek Wyslouch,*First Results from Pb+Pb collisions at the LHC*,(2012),http://arxiv.org/abs/1202.3233